Frequency of Seyfert Type Transitions in a Sample of 102 Local Active Galactic Nuclei

Jordan Runco

A Thesis presented for the degree of
Physics

CAL POLY
SAN LUIS OBISPO

Department of Physics
California Polytechnic State University
San Luis Obispo, California

June 2015

Abstract

A sample of ∼100 type-1 local ($0.02 \leq z \leq 0.1$) active galaxies (AGNs) was selected from the Sloan Digital Sky Survey with black hole masses $M_{\rm BH} > 10^7 M_{\odot}$ and re-observed using the Keck 10-m telescope to study the local scaling relations between $M_{\rm BH}$ and the host galaxy properties. As a side product, the data provides insight into any changes of the broad-line region within the 3-9 year time-frame covered by the two sets of spectra. The variability of the broad Hβ emission line is of particular interest to us, not only because it is used to estimate $M_{\rm BH}$, but also because its presence and width acts as a classifier for the so-called Seyfert-type of these galaxies. Roughly 44% of the sample show significant broad-line variability with a change in Seyfert classification, questioning the standard unified model for active galaxies in which the AGN type depends only on viewing angle. The observed type change cannot simply be explained by a drop in black hole accretion rate, as traced by the AGN power-law continuum. Also, we do not find evidence for obscuration to play the dominant role in the observe change in Hβ line width. More data are needed to determine the origin of the line profile changes. While similar dramatic transitions have been reported in the literature, our study is the first to provide statistical information.

Contents

1 Introduction **1**

1.1 Overview of Active Galactic Nuclei 1

1.2 Measuring Black Hole Mass 4

1.3 Outline of Thesis 7

2 Sample Selection, Observations, and Data Reduction **8**

2.1 Sample Selection 8

2.2 Observations 8

2.2.1 SDSS 8

2.2.2 Keck 8

2.3 Data Reduction 9

2.4 Difference Between Keck and SDSS Observations 9

3 Data Analysis and Results **14**

3.1 Qualitative Analysis 14

3.1.1 Unsubtracted Spectra 14

3.1.2 Subtracted Spectra 14

3.1.3 Seyfert-Type Change 15

3.2 Quantitative Analysis 20

3.2.1 Hβ Fitting 20

3.2.2 Continuum Powerlaw 25

3.2.3 Hβ Line Flux Variations 26

3.2.4 FeII Emission Line Subtraction 28

4 Discussion of Results **30**

4.1 Seyfert-Type Change in the Sample 30

4.2 Observations from the Data 30

4.3 Comparison to Literature 31

4.3.1 Comparison to Scott et al. 31

4.3.2 Comparison to Other Literature 32

5 Conclusions **34**

6 Acknowledgements **36**

Bibliography **37**

Appendix **39**

A Qualitative Analysis Plots **39**

A.1 Unsubtracted Spectra 39

A.2 Subtracted Spectra 47

B Hβ Fitting **51**

B.1 SDSS 52

B.2 Keck 57

C Continuum Powerlaw Fitting **62**

List of Figures

1.1 Unified model and viewing orientations for type-1 and type-2 Seyfert galaxies. 2
1.2 Type-1 and type-2 Seyfert spectra. 3
1.3 Model of broad-line region for reverberation mapping. 5
1.4 Example of Hβ width used to calculate $M_{\rm BH}$. 5
1.5 Example of reverberation mapping showing variability of Hβ and [OIII] lines. 6
1.6 Empirical relation between BLR size and the luminosity of the 5100Å line. 7

3.1 Magnitude of Seyfert-type transitions. 19
3.2 Time between observations vs. magnitude of Seyfert-type change. 19
3.3 Second moment of the model to the broad Hβ line, $\sigma_{\rm H\beta}$, SDSS vs. Keck. 21
3.4 Full-Width at Half Maximum SDSS vs. Keck. 22
3.5 Logarithmic $M_{BH}/M_{\odot}$ SDSS vs. Keck in units of $M_{\odot}$. 22
3.6 Second moment of the data to the broad Hβ line SDSS vs. Keck. 23
3.7 Flux ratio between the narrow Hβ line and [OIII] lines. 23
3.8 Flux ratio between the narrow Hβ line and broad Hβ line. 24
3.9 Change in $\sigma_{\rm H\beta}$ vs. change in powerlaw exponent. 25
3.10 Change in $\sigma_{\rm H\beta}$ vs. change in H$\beta_{\rm narrow}$/H$\beta_{\rm broad}$ flux ratio. 26
3.11 Change in powerlaw exponent vs. change in Hβ/[OIII] flux ratio. 27
3.12 Change in powerlaw exponent vs. change in Hβ_{narrow}/Hβ_{broad} flux ratio. 27
3.13 Same plot as Figure 3.3 but objects marked for FeII subtraction. 28
3.14 Same plot as Figure 3.9 but objects marked for FeII subtraction. 29

A.1 15 objects from the unsubtracted data set. 40
A.2 Same as Figure A.1 for 15 different objects. 41
A.3 Same as Figure A.1 for 15 different objects. 42
A.4 Same as Figure A.1 for 15 different objects. 43
A.5 Same as Figure A.1 for 15 different objects. 44
A.6 Same as Figure A.1 for 15 different objects. 45
A.7 Same as Figure A.1 for 12 different objects. 46
A.8 40 objects from the subtracted data set. 48

A.9 Same as Figure A.8 for 40 different objects. 49
A.10 Same as Figure A.8 for 22 different objects. 50

B.1 Hβ and [OIII] line fitting for 40 SDSS objects. 52
B.2 Same as Figure B.1 for 39 different objects. 53
B.3 Hβ and [OIII] line fitting for 40 Keck objects. 57
B.4 Same as Figure B.3 for 39 different objects. 58

List of Tables

1.1 Seyfert-type classifications. 3

2.1 Coordinates, redshift, and exposure times for all 102 objects in the sample. 13

3.1 Seyfert-type classifications for sample. 18
3.2 Broad Hβ fitting statistics. 24
3.3 Continuum powerlaw fitting statistics. 25
3.4 Change in $\sigma_{\mathrm{H}\beta}$ vs. change in $\mathrm{H}\beta_{\mathrm{narrow}}/\mathrm{H}\beta_{\mathrm{broad}}$ flux ratio fitting statistics. 26
3.5 Powerlaw vs. Hβ flux statistics. 28
3.6 FeII subtraction statistics. 29

B.1 Broad Hβ fitting data for 79 SDSS objects. 56
B.2 Broad Hβ fitting data for 79 Keck objects. 61

C.1 Continuum powerlaw exponent fitting data for all SDSS and Keck objects in our sample. 65

Chapter 1

Introduction

When first discovered, the brightest objects in the universe were a mystery to astronomers because they are approximately the size of our solar system, but have the luminosity of millions of stars. These objects are now known as Active Galactic Nuclei (AGN). In our current understanding, every AGN resides in the center of a host galaxy, but can have the luminosity to outshine its host galaxy.

1.1 Overview of Active Galactic Nuclei

This summary of AGNs refers to "An Introduction to Active Galactic Nuclei" (Peterson 1997). There are many components that make up an AGN; Figure 1.1 below provides a diagram of this. At the core is a supermassive ($10^7 M_\odot$ [1]) black hole (BH) with an accretion disk of gas and dust orbiting it. All matter in the accretion process falls on to a disk in order to conserve angular momentum; the matter accreted on to this disk is very hot. The emission spectra observed from the accretion disk are thermal, like blackbody spectra, with a thermal gradient of higher temperatures in the inner regions. The sum of these blackbody spectra results in a powerlaw in the UV-optical regime that rises towards shorter wavelengths. Just outside the accretion disk is the broad line region (BLR). Groups of gas clouds reside in this region and the clouds are very dense and numerous with high orbital velocities (500km s^{-1} - 5000km s^{-1}). Light from the accretion disk ionizes gas in the BLR, in particular hydrogen. The ionized BLR gas re-emits this light upon recombination in the form of Balmer lines, which we observe. The fast orbital speeds of the BLR lead to some particles moving away from Earth increasing the wavelength of light (red-shift) while other particles move towards Earth shortening the wavelength (blue-shifted). The combination of red-shifted and blue-shifted light causes emission lines to become wider, and this process is called Doppler broadening. Outside of the BLR is a ring of gas and dust called the dusty torus that orbits the black hole on the same plane as the accretion disk. The narrow line region (NLR) is farther away from the BH than the BLR and dusty torus, but contains gas clouds with many of the same properties as the BLR. NLR gas clouds orbit at smaller speeds (200km s^{-1} - 900km s^{-1}) than clouds in

[1] $M_\odot = 1.99 \times 10^{30}$kg

the BLR due to their larger distance to the BH. The smaller speeds of NLR clouds lead to less Doppler broadening, resulting in narrower emission lines. The last part of an AGN is the jet, which contains sub-relativistic electrons moving along magnetic field lines. These accelerated charged particles are shot out of the center of the AGN and give off light in the radio, called synchrotron radiation. Accretion onto the BH is not constant in time, causing the amount of light given off to vary. This affects both the powerlaw and ionized emission from the BLR, which respond to the accretion emission, making AGNs variable.

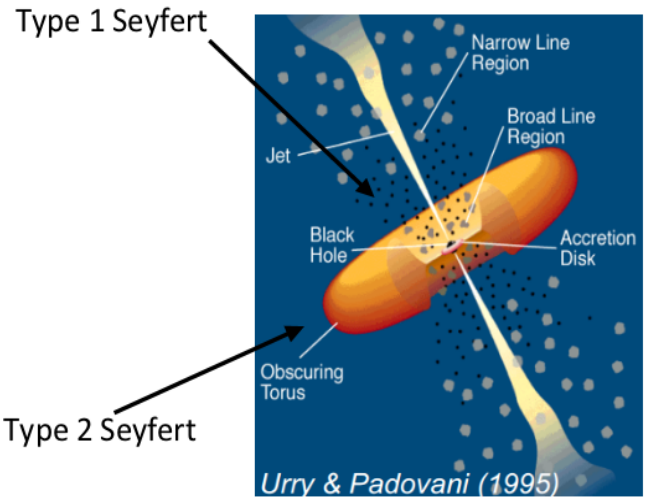

Figure 1.1: The current model of AGNs that showcases the viewing orientations for type-1 and type-2 Seyfert galaxies. (Urry and Padovani 1995)

The two largest subclasses of AGNs are Seyfert galaxies and quasars. Quasars are much brighter and outshine their host galaxy, while the host galaxy can be easily observed in Seyferts. For that reason, this thesis focuses on Seyfert galaxies. Most Seyfert galaxies are spiral galaxies, and Seyferts are broken up into categories ranging from type-1 to type-2 with several subcategories in-between. Seyfert-1 galaxies have both broad and narrow emission lines while Seyfert-2 only emit narrow lines. Type-1.5, 1.8, 1.9 Seyfert galaxies show intermediate properties of both type-1 and 2 Seyfert galaxies. Figure 1.2 below gives examples of Seyfert-1 and Seyfert-2 spectra.

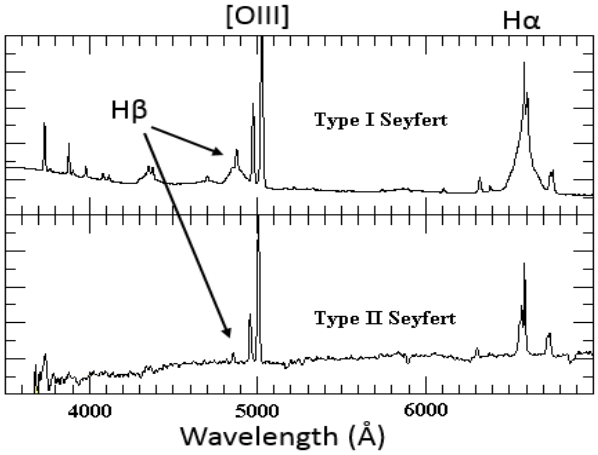

Figure 1.2: An example of Seyfert-1 and Seyfert-2 spectra highlighting their differences. The broad Hβ and Hα lines are only present in type-1 Seyferts. The strong [OIII] emission line is narrow in both cases. Flux is in arbitrary units and wavelength is in Å. (Morgan 2002)

A theory that all Seyfert galaxies are intrinsically the same just viewed at different angles has been suggested, called the unified model. Type-2 Seyfert galaxies do not possess broad emission lines like type-1 Seyferts. The unified model suggests that the broad lines exist but are being obscured by the dusty torus absorbing the broad lines. Type-2 Seyferts are viewed along the same plane as the dusty torus, while Seyfert-1 are viewed "face-on", so both the accretion disk and the BLR are visible (refer to Figure 1.1 above for the viewing angles for Seyfert-1 and 2). Intermediate types-1.5, 1.8, and 1.9 are viewed along the edges of the dusty torus where it is not optically thick enough to fully block the broad Hβ line (refer to Table 1.1 below for Seyfert-type classifications). The Balmer series, mainly the Hα and Hβ lines, are generally used to classify Seyfert-type. The unified model implies that the AGN's orientation to us determines which lines can be observed from Earth.

Seyfert-Type Classifications	
Type	Description
Type-1	Both broad and narrow components in all Balmer lines.
Type-1.5	Broad and narrow components can be identified in Hα and Hβ. Broad component of higher order Balmer lines is weakening.
Type-1.8	Broad Hβ is weak but detectable. No higher order Balmer lines have a broad component.
Type-1.9	Shows broad Hα but no higher order Balmer lines have a broad component.
Type-2	No broad emission lines.

Table 1.1: Seyfert-type classifications based on the strength of the Hβ and Hα lines. (Osterbrock, D.E. 1977; 1981)

1.2 Measuring Black Hole Mass

Three relationships between the mass of a BH ($M_{\rm BH}$) and the host galaxy have been found: spheroid luminosity L_{sph} (Kormendy & Richstone 1995), spheroid mass M_{sph} (Magorrian et al. 1998), and spheroid stellar velocity dispersion σ (Gebhardt et al. 2000; Ferrarese & Merritt 2000), a measurement of stellar line broadening which gives us an idea about how the stars are orbiting in the galaxy, and ultimately the mass of the spheroid. The relations between $M_{\rm BH}$ and the properties of the host galaxy they live in is surprising given the different scales involved − the gravitational sphere of influence of the BH is on the pc [2] scale while the bulge is on the kpc scale. In other words, the BH's sphere of influence is a factor of 1000 smaller than the size of the bulge around the BH. Thus, the $M_{\rm BH}$ scaling relations are not necessarily expected. They can be explained if BHs and their host galaxies are related through a feedback mechanism that controls mutual growth. For AGNs, high energetic gas is expelled out into the host galaxy (e.g. through jets), which heats up material and limits star formation. This feedback also limits BH growth, as matter that could be accreted on to the BH is expelled into the host galaxy. Another origin of these relations could be the mutual growth of BHs and their host galaxies in a process called galaxy merging, where two galaxies and their BHs merge into one bigger galaxy with a more massive BH (Peterson 1997).

One method for calculating $M_{\rm BH}$ is to directly measure kinematics of stars or gas within the gravitational sphere of influence of the BH. This requires the BH's gravitational sphere of influence to be spatially resolved, restricting this method to the local universe. For galaxies outside the local universe, there are two techniques for calculating $M_{\rm BH}$ for active galaxies called reverberation mapping (RM) (Wandel et al. 1999; Kaspi et al. 2000, 2005; Bentz et al. 2006, 2013) and the single-epoch method. RM is the primary technique to calculate $M_{\rm BH}$ by obtaining the size and velocity of the BLR. Continuum variations cause changes to BLR emission lines. These changes originate from the center of the AGN and spread out across the BLR as a function of time delay. Time delay is due to light time-travel effects within the BLR, and the size of the BLR is estimated from the average time delay.

[2] pc = 3.26ly = 3.09x10^{16}m

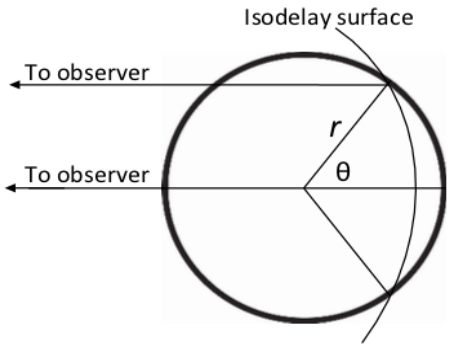

Figure 1.3: Changes to the BLR emission originate from the accretion disk and travel out to the BLR. The isodelay surface for an arbitrary time is given; the intersection of this surface and the BLR ring shows the clouds that are observed to be responding at this particular time. This model assumes that the BLR is a uniform spherical shell of radius r. (Peterson 1997)

The velocity of the BLR clouds is obtained from the width of the broad Hβ line.

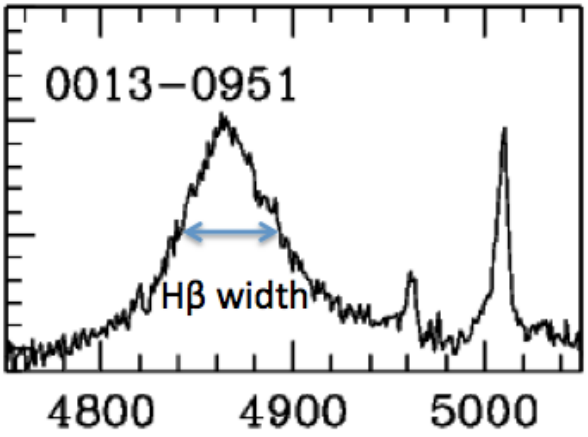

Figure 1.4: Example of Hβ witdh used to calculate $M_{\rm BH}$.

Taken together, assuming Keplerian motion of the BLR clouds, $M_{\rm BH}$ can be estimated as:

$$M_{BH} = \frac{fRv_{BLR}^2}{G} \tag{1.2.1}$$

where f is a constant based on the geometry of the BLR called the virial coefficient, $R_{\rm BLR}$ is the average BLR radius found from RM, v is the velocity found from the broad Hβ line, and G is the gravitational constant (Peterson 1997). The main uncertainty originates from the unknown geometry of the BLR and the virial coefficient, which is estimated to be about 0.4 dex. Recent studies have suggested that modeling RM data directly and constraining the geometry and kinematics of the BLR has eliminated the need for the virial coefficient in the equation above (Brewer et al. 2011; Pancoast et al. 2011, 2012, 2014). Figure 1.5 is an example of RM for the Hβ and 4960Å [OIII] emission lines for galaxy NGC 4151 (Bentz et al. 2006).

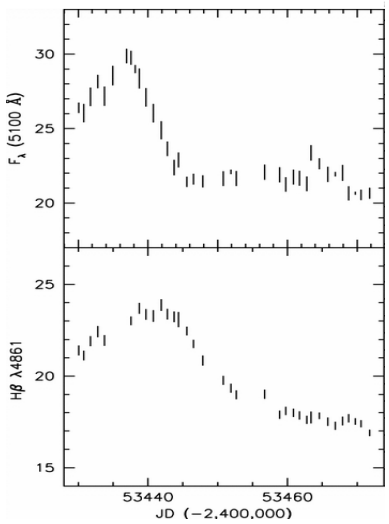

Figure 1.5: Example of RM of the Hβ emission line for NGC 4151. This shows the variability of lightcurves for the Hβ line and 5100Å continuum originating in the accretion disk over the course of approximately 50 days. (Bentz et al. 2006)

The single epoch is a secondary method to find $M_{\rm BH}$ that uses an empirical relationship of $R_{\rm BLR}$ and the continuum luminosity at the 5100Å to determine $R_{\rm BLRf}$. In the single epoch method, all that is needed to estimate $M_{\rm BH}$ for an AGN is the continuum luminosity of the AGN and the width of the Hβ line which is taken from one single spectrum (hence the name single epoch). This is the method used throughout this thesis. The downside of this method is that the uncertainty involved is even larger than from RM. Velocity once again comes from the broad Hβ line, the $M_{\rm BH}$ can be estimated:

$$M_{BH} = \frac{f L_{5100}^{0.5} v_{BLR}^2}{G} \tag{1.2.2}$$

where L_{5100} is the luminosity at 5100Å. Figure 1.6 shows the correlation between L_{5100} and BLR radius.

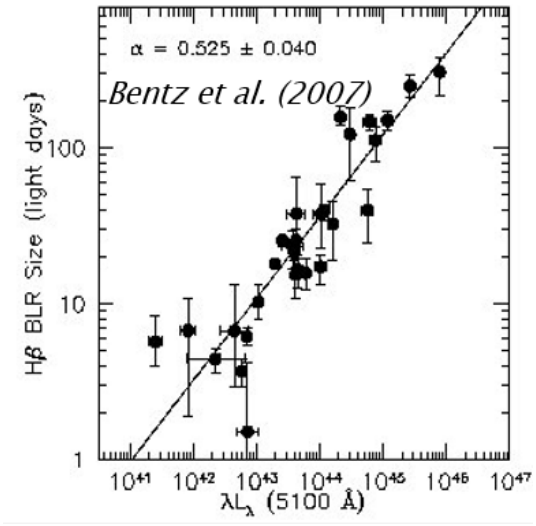

Figure 1.6: Empirical relation between BLR size determined from RM of the Hβ line and the luminosity of the 5100Å continuum. (Bentz et al. 2007)

1.3 Outline of Thesis

To build a local sample of the $M_{\rm BH}$-σ scaling relations for active galaxies, Dr. Vardha N. Bennert selected $\sim$100 local ($0.02 \leq z \leq 0.09$) Seyfert-1 galaxies with $M_{BH} > 10^7 M_{\odot}$ from the Sloan Digital Sky Survey (SDSS). Spectra for all objects were taken using the Keck-10m telescope (more on selection process and instrumental details in the next section). This is a unique sample because each object has been measured twice at separate times (SDSS and Keck, about 3-9 years apart), allowing us to inspect how the spectra of these objects changed. Former Cal Poly student Rebecca Rosen noticed that not all Keck spectra have broad Hβ lines while being present in SDSS (Rosen et al. 2012), and Bryan Scott proceeded to inspect eight objects that show no broad Hβ in Keck (Scott et al. 2013). This paper builds upon what Bryan studied and inspects changes to the continuum spectra and broad Hβ line of the entire sample and how this affects their classification. The Hβ line will primarily be focused on because it is a broad line originating in the BLR and it is useful for calculating $M_{\rm BH}$ as stated above. The width of the broad Hβ emission line is also used to determine the Seyfert-type. We look for a relationship between AGN powerlaw and the broad Hβ line to test if the AGN powerlaw is the driving force behind the broad Hβ width. Also, we look for evidence of dust obscuration causing the observed changes.

This senior thisis is organized in the following manner. Section 2 summarizes the sample selection, data reduction, and observations. Section 3 describes derived quantities and data results. Section 4 includes a discussion of results and a comparison to similar papers. Lastly, section 5 is a conclusion for this paper. Appendix A provides continuum fitting for the broad Hβ line for all 102 SDSS and Keck spectra. Appendix B provides broad Hβ fits for 79 SDSS and Keck objects. Appendix C provides values of the continuum powerlaw exponent for all SDSS and Keck objects in the sample. Throughout the paper, a Hubble constant of $H_{\rm O} = 70$ km s^{-1} Mpc^{-1}, $\Omega_{\lambda} = 0.7$ and $\Omega_{M} = 0.3$ will be assumed.

Chapter 2

Sample Selection, Observations, and Data Reduction

2.1 Sample Selection

A sample of ∼100 type-1 local ($0.02 \leq z \leq 0.09$) AGNs were selected from the Sloan Digital Sky Survey (SDSS) DR6 data release with $M_{BH} > 10^7 M_{\odot}$ and a broad Hβ emission line. The sample is limited to the local universe so that the host galaxies are well resolved and stellar kinematics can be measured using the [CaII] triplet (8500.36Å, 8544.44Å, and 8664.52Å) lines in the optical.

2.2 Observations

2.2.1 SDSS

SDSS images and spectra are obtained using a 2.5-m ground-based telescope with a 3" diameter circular optical fiber and are available through the SDSS archive. SDSS spectra cover a wavelength range of 3800Å to 9200Å, and has a resolution of 170 km s^{-1}. The exposure time for all SDSS spectra is 54 seconds. ("Survey Instruments" 2003)

2.2.2 Keck

These same objects were observed between January 2009 and March 2010 with the Keck-10m telescope using the Low Resolution Imaging Spectrometer (LRIS) and a 1" wide slit. This slit is aligned along the major axis of each galaxy which is determined from the SDSS images. The D560 dichroic is used for data taken in 2009 and the D680 dichroic is used for data taken in 2010. A 600/4000 grism is used for the blue side of the spectra resulting in an instrumental resolution of 90km s^{-1} and wavelength range of 3200-5600Å. A 831/8200 grating is used for the red side resulting in a central wavelength of 8950Å and an instrumental resolution of 45 km s^{-1}. In this thesis, the red Keck spectra are not used. Typical exposure times for this sample range between 600-1200 seconds. (Bennert et al. 2011)

2.3 Data Reduction

SDSS data retrieved from the SDSS archive is already reduced, and the spectra are absolutely flux calibrated. Keck data is reduced using a Python script following standard procedures such as bias and flat field correction, removing cosmic rays, and wavelength calibration using arc lamps for blue and sky emission lines for red. A0V Hipparcos stars are used to correct for telluric absorption lines and relative flux calibration. My task is to take the Keck and SDSS data one step further by subtracting out all of the stellar absorption lines and the powerlaw from the AGN continuum, leaving only broad and narrow emission lines originating from the AGN. A Python script is used to both fit a linear combination of known stellar profiles and fit a powerlaw to the continuum. Masking the broad lines gives an accurate measurement of the stellar continuum. Subtracting the underlying stellar absorption lines of the host galaxy leaves only the AGN spectra. This is done to more accurately measure the width and strength of the remaining emission lines. Those spectra are referred to throughout the thesis as the subtracted data sets. A copy of the data that is not stellar and powerlaw subtracted is also kept, which are the unsubtracted data sets. This thesis utilizes and discusses a total of four data sets throughout this paper: Keck subtracted, Keck unsubtracted, SDSS subtracted, and SDSS unsubtracted. All four sets of data contain the exact same objects and each specific set is used for different purposes.

2.4 Difference Between Keck and SDSS Observations

In this thesis, we compare spectra from two different telescopes, SDSS and Keck. We here discuss some of the important differences.

1. Aperture: SDSS spectra are obtained using a 2.5-m ground-based telescope with an circular fiber 3" in diameter, while the Keck spectra are taken using the LRIS at Keck 10-m telescope with a 1" x 2" rectangle slit. This could lead to a difference in observed flux; however, the Keck slit is aligned along the major axis of the host galaxy determined by SDSS to minimize this uncertainty.

2. Exposure times: Typical values for Keck range from 600 to 1200 seconds; all SDSS images are 54 seconds.

3. Time taken: Below is a table of observation times for Keck and SDSS objects. The SDSS spectra, by selection, were taken first, and depending on the object, between 3-9 years earlier than the Keck spectra. The largest time difference between observations is 9.13 years while the smallest is 2.57 years. The average time between observations is 6.44 ± 1.84 years.

4. SDSS spectra are absolute flux calibrated but Keck spectra are not since observing conditions were typically not photometric.

5. The spectral ranges and resolution of SDSS and Keck are different. SDSS spectra cover 3800Å to 9200Å with a resolution of 170 km s^{-1} while Keck spectra cover approximately 3600Å to 5400Å

and has a resolution of 90 km s^{-1} for the blue side of the spectra and has a resolution of 45 km s^{-1} with a central wavelength of 8950Å for the red side. Note that we are only considering the blue Keck spectra in this thesis.

In order to compare the two data sets given these differences in observations, Keck spectra were re-binned to match the spectral resolution of SDSS spectra. Also, we make the assumption that the [OIII] 5007Å emission line flux is identical in both data sets. This assumption is justified by the fact that the NLR is not variable on the observed timescales; however, it assumes that both spectra integrate the same [OIII] emission over the same area, which is a good first order approximation, but not necessarily correct given the different regions covered with the fiber vs. long-slit spectra. Finally, note that in all cases, the AGN 5100Å luminosity needed to estimate $M_{\rm BH}$ is derived from image decomposition from the SDSS images (see Bennert et al. 2015 for details), taken at yet another different time. Given that the AGN powerlaw is known to be variable, that could introduce a bias in our analysis. These caveats have to be taken into consideration when comparing the spectra, but this is the best approximation we can do given the data we have. As I will discuss later, especially changes in the broad Hβ profile cannot be explained by any of these caveats.

Table of Observations

Object	I.D.	RA	Dec	z	Exp. time Keck [s]	Time taken Keck	Time taken SDSS	Time between observation (years)
0013-0951	L71	00 13 35.3	−09 51 20.9	0.0615	600	09-20-2009	08-17-2001	8.09
0026+0009	L5	00 26 21.29	+00 09 14.9	0.0600	1600	09-20-2009	08-26-2000	9.07
0038+0034	L73	00 38 47.96	+00 34 57.5	0.0805	600	09-20-2009	09-06-2000	9.04
0109+0059	L74	01 09 39.01	+00 59 50.4	0.0928	600	09-20-2009	09-07-2000	9.04
0121-0102	L11	01 21 59.81	−01 02 24.4	0.0540	1200	01-21-2009	09-02-2000	8.39
0150+0057	L76	01 50 16.43	+00 57 01.9	0.0847	600	09-20-2009	09-06-2000	9.04
0206-0017	L2	02 06 15.98	−00 17 29.1	0.0430	1200	01-22-2009	09-25-2000	8.33
0212+1406	L77	02 12 57.59	+14 06 10.0	0.0618	600	09-20-2009	12-05-2000	8.79
0301+0110	L78	03 01 24.26	+01 10 22.5	0.0715	600	09-20-2009	09-30-2000	8.97
0301+0115	L79	03 01 44.19	+01 15 30.8	0.0747	600	09-20-2009	09-30-2000	8.97
0310-0049	L80	03 10 27.82	−00 49 50.7	0.0801	600	09-20-2009	12-15-2001	7.76
0336-0706	L9	03 36 02.09	−07 06 17.1	0.097	2400	09-20-2009	12-31-2000	8.72
0353-0623	L6	03 53 01.02	−06 23 26.3	0.076	1200	01-22-2009	12-30-2000	8.06
0731+4522	L81	07 37 26.68	+45 22 17.4	0.0921	600	09-20-2009	11-05-2004	4.87
0735+3752	L82	07 35 21.19	+37 52 01.9	0.0962	600	09-20-2009	11-29-2000	8.81
0737+4244	L83	07 37 03.28	+42 44 14.6	0.0882	600	09-20-2009	01-31-2004	5.64

Continued on next page

Table2.1– *Continued from previous page*

Object	I.D.	RA	Dec	z	Exp. time Keck [s]	Time taken Keck	Time taken SDSS	Time between observations (years)
0802+3104	L1	08 02 43.40	+31 04 03.3	0.041	1200	01-21-2009	01-02-2003	5.97
0811+1739	L114	08 11 10.28	+17 39 43.9	0.0649	2700	03-15-2010	12-18-2004	5.24
0813+4608	L10	08 13 19.34	+46 08 49.5	0.054	1200	01-14-2010	11-29-2000	9.13
0831+0521	L208	08 11 10.28	+17 39 43.9	0.035	600	03-15-2010	01-07-2003	7.18
0845+3409	L126	08 45 56.67	+34 09 36.3	0.0655	3600	03-14-2010	02-02-2003	7.11
0846+2522	L4	08 46 54.09	+25 22 12.3	0.051	1200	01-22-2009	12-19-2004	4.09
0847+1842	L8	08 47 48.28	+18 24 39.9	0.085	1200	01-21-2009	12-07-2005	3.10
0854+1741	L130	08 54 39.25	+17 41 22.5	0.0654	600	03-15-2010	12-25-2005	4.22
0857+0528	L19	08 57 37.77	+05 28 21.3	0.0586	600	01-15-2010	01-31-2003	6.96
0904+5536	L20	09 04 36.95	+55 36 02.5	0.0371	600	03-14-2010	12-30-2000	9.20
0909+1330	L21	09 09 02.35	+13 30 19.4	0.0506	600	01-14-2010	04-01-2006	3.79
0921+1017	L22	09 21 15.55	+10 17 40.9	0.0392	700	01-14-2010	02-15-2004	5.91
0923+2254	L23	09 23 43.00	+22 54 32.7	0.0332	600	01-15-2010	12-23-2005	4.06
0923+2946	L138	09 23 19.73	+29 46 09.1	0.0625	600	01-15-2010	01-19-2005	4.99
0927+2301	L24	09 27 18.51	+23 01 12.3	0.0262	600	01-15-2010	12-26-2005	4.05
0932+0233	L26	09 32 40.55	+02 33 32.6	0.0567	600	01-14-2010	02-25-2001	8.88
0932+0405	L27	09 32 59.60	+04 05 06.0	0.0590	600	01-14-2010	12-21-2001	8.07
0936+1014	L143	09 36 41.08	+10 14 15.7	0.0600	3600	03-15-2010	12-20-2003	6.23
0938+0743	L28	09 38 12.27	+07 43 40.0	0.0218	600	01-14-2010	04-04-2003	6.78
0948+4030	L29	09 48 38.43	+40 30 43.5	0.0469	900	01-15-2010	03-11-2003	6.85
1002+2648	L30	10 02 18.79	+26 48 05.7	0.0517	600	01-15-2010	01-22-2006	3.98
1029+1408	L155	10 29 25.73	+14 08 23.2	0.0608	600	01-15-2010	03-11-2004	5.85
1029+2728	L31	10 29 01.63	+27 28 51.2	0.0377	600	01-15-2010	02-28-2006	3.88
1029+4019	L156	10 29 46.80	+40 19 13.8	0.0672	600	01-14-2010	01-29-2004	5.96
1038+4658	L157	10 38 33.42	+46 58 06.0	0.0631	600	01-14-2010	12-12-2002	7.09
1042+0414	L32	10 42 52.94	+04 14 41.1	0.0524	1200	04-16-2009	03-06-2002	7.11
1043+1105	L33	10 43 26.47	+11 05 24.3	0.0475	600	04-16-2009	04-20-2004	4.99
1049+2451	L34	10 49 25.39	+24 51 23.7	0.0550	600	04-16-2009	02-26-2006	3.13
1058+5259	L162	10 58 28.76	+52 59 29.0	0.0676	600	01-14-2010	01-13-2003	7.00
1101+1102	L35	11 01 01.78	+11 02 48.8	0.0355	600	04-16-2009	04-24-2004	4.98
1104+4334	L36	11 04 56.03	+43 34 09.1	0.0493	600	01-14-2010	02-18-2004	5.91
1110+1136	L37	11 10 45.97	+11 36 41.7	0.0421	3600	03-15-2010	03-14-2004	6.00

Continued on next page

Table2.1– *Continued from previous page*

Object	I.D.	RA	Dec	z	Exp. time Keck [s]	Time taken Keck	Time taken SDSS	Time between observations (years)
1116+4123	L13	11 16 07.65	+41 23 53.2	0.021	850	04-15-2009	12-30-2003	5.29
1118+2827	L38	11 18 53.02	+28 27 57.6	0.0599	900	01-15-2010	02-27-2006	3.88
1132+1017	L14	11 32 49.28	+10 17 47.4	0.044	600	01-15-2010	05-22-2003	6.65
1137+4826	L39	11 37 04.17	+48 26 59.2	0.0541	600	01-14-2010	01-03-2003	7.03
1139+5911	L174	11 39 08.95	+59 11 54.6	0.0612	600	01-14-2010	05-15-2002	7.67
1140+2307	L40	11 40 54.09	+23 07 44.4	0.0348	1200	01-15-2010	05-21-2006	3.66
1143+5941	L177	11 43 44.30	+59 51 12.4	0.0629	3000	03-14-2010	05-17-2002	7.82
1144+3653	L15	11 44 29.88	+36 53 08.5	0.038	600	04-16-2009	03-13-2005	4.09
1145+5547	L41	11 45 45.18	+55 47 59.6	0.0534	3600	03-14-2010	04-30-2003	6.87
1147+0902	L180	11 47 55.08	+09 02 28.8	0.0688	600	01-15-2010	05-01-2003	6.71
1205+4959	L187	12 05 56.01	+49 59 56.4	0.0630	600	01-14-2010	06-17-2002	7.58
1206+4244	L42	12 06 26.29	+42 44 26.1	0.0520	1100	03-14-2010	04-25-2004	5.88
1210+3820	L43	12 10 44.27	+38 20 10.3	0.0229	600	04-16-2009	04-13-2005	4.01
1216+5049	L44	12 16 07.09	+50 49 30.0	0.0308	900	03-14-2010	05-19-2002	6.82
1223+0240	L45	12 23 24.14	+02 40 44.4	0.0235	600	03-15-2010	01-09-2002	8.18
1228+0951	L210	12 28 11.41	+09 51 26.7	0.0640	600	03-15-2010	04-02-2003	6.95
1231+4504	L196	12 31 52.04	+45 04 42.9	0.0621	1200	01-15-2010	02-27-2004	5.88
1241+3722	L197	12 41 29.42	+37 22 01.9	0.0633	800	01-15-2010	04-02-2006	3.79
1246+5134	L202	12 46 38.74	+51 34 55.9	0.0668	600	01-15-2010	04-15-2002	7.75
1250-0249	L46	12 50 42.44	−02 49 31.5	0.0470	1200	04-16-2009	03-29-2001	8.05
1306+4552	L47	13 06 19.83	+45 52 24.2	0.0507	3600	03-14-2010	04-22-2004	5.89
1307+0952	L48	13 07 21.93	+09 52 09.3	0.0490	2400	03-15-2010	05-29-2006	3.79
1312+2628	L204	13 12 59.59	+26 28 24.0	0.0604	2700	03-14-2010	02-28-2006	4.04
1313+3653	L213	13 13 48.96	+36 53 57.9	0.0667	600	03-14-2010	03-21-2006	3.98
1323+2701	L49	13 23 10.39	+27 01 40.4	0.0559	700	04-16-2009	03-01-2006	3.13
1353+3951	L207	13 53 45.93	+39 51 01.6	0.0626	600	03-14-2010	02-26-2004	6.05
1355+3834	L50	13 55 53.52	+38 34 28.5	0.0501	300	04-16-2009	03-31-2005	4.04
1405-0259	L51	14 05 14.86	−02 59 01.2	0.0541	1600	04-16-2009	06-18-2002	6.83
1416+0317	L52	14 16 30.82	+01 37 07.9	0.0538	2700	03-15-2010	03-26-2001	8.97
1419+0754	L53	14 19 08.30	+07 54 49.2	0.0558	900	04-16-2009	06-12-2005	3.84
1423+2720	L209	14 23 38.43	+27 20 09.7	0.0639	1200	03-14-2010	05-26-2006	3.80
1434+4839	L54	14 34 52.45	+48 39 42.5	0.0365	600	04-16-2009	04-04-2003	6.03

Continued on next page

Table2.1– *Continued from previous page*

Object	I.D.	RA	Dec	z	Exp. time Keck [s]	Time taken Keck	Time taken SDSS	Time between observations (years)
1505+0342	L56	15 05 56.55	+03 42 26.3	0.0358	1200	03-15-2010	05-26-2001	8.80
1535+5754	L57	15 35 52.40	+57 54 09.3	0.0304	1200	04-15-2009	03-14-2002	7.09
1543+3631	L214	15 43 51.49	+36 31 36.7	0.0672	1200	03-15-2010	08-24-2003	6.56
1545+1709	L58	15 45 07.53	+17 09 51.1	0.0481	1200	04-15-2009	06-03-2006	2.57
1554+3238	L59	15 54 17.42	+32 38 37.6	0.0483	1200	04-15-2009	07-05-2003	5.78
1557+0830	L60	15 57 33.13	+08 30 42.9	0.0465	1200	04-15-2009	08-11-2004	4.68
1605+3305	L61	16 05 02.46	+33 05 44.8	0.0532	1200	04-15-2009	05-17-2004	4.91
1606+3324	L62	16 06 55.94	+33 24 00.3	0.0585	1200	04-15-2009	05-19-2004	4.91
1611+5211	L63	16 11 56.30	+52 11 16.8	0.0409	1200	04-15-2009	05-22-2001	7.95
1636+4202	L205	16 36 31.28	+42 02 42.5	0.0610	1200	03-14-2010	06-23-2001	8.72
1647+4442	L64	16 47 21.47	+44 42 09.7	0.0253	4200	03-14-2010	05-22-2001	8.81
1655+2014	L88	16 55 14.21	+20 12 42.0	0.0841	600	09-20-2009	06-13-2004	5.27
1708+2153	L91	17 08 59.15	+21 53 08.1	0.0722	600	09-20-2009	06-21-2004	5.25
2116+1102	L96	21 16 46.33	+11 02 37.3	0.0805	700	09-20-2009	07-13-2002	7.19
2140+0025	L99	21 40 54.55	+00 25 38.2	0.0838	600	09-20-2009	07-10-2002	7.20
2215-0036	L100	22 15 42.29	−00 36 09.6	0.0992	600	09-20-2009	09-04-2000	9.04
2221-0906	L102	22 21 10.83	−09 06 22.0	0.0912	600	09-20-2009	10-21-2001	7.92
2222-0819	L103	22 22 46.61	−08 19 43.9	0.0821	700	09-20-2009	10-24-2001	7.91
2233+1312	L106	22 33 38.42	+13 12 43.5	0.0934	800	09-20-2009	09-04-2002	7.04
2254+0046	L108	22 54 52.24	+00 46 31.4	0.0907	600	09-20-2009	09-02-2000	9.05
2327+1524	L70	23 27 21.97	+15 24 37.4	0.0458	600	09-20-2009	11-25-2001	7.82
2351+1552	L109	23 51 28.75	+15 52 59.1	0.0963	600	09-20-2009	11-13-2001	7.85

Table 2.1: Coordinates, redshift, and exposure times for all 102 objects in the sample. The exposure time for all SDSS spectra is 54 seconds. The average time between observations is 6.44 ± 1.84 years.

Chapter 3

Data Analysis and Results

3.1 Qualitative Analysis

To get a first idea of trends in the data, I started by preforming a qualitative analysis and inspected the spectra by eye to look for changes in the Hβ line and continuum emission. In the next section, I discuss a more quantitative analysis, including fitting the data.

3.1.1 Unsubtracted Spectra

Since the continuum of the AGN powerlaw could be the driving force in changes in the Hβ line profile, I first inspected the change of the continuum spectrum for each object over the approximately 3-9 year difference between Keck and SDSS. This is accomplished by overlaying the unsubtracted spectra of Keck and SDSS on the same plot for each object. The plots for the 102 objects are in Appendix A.1 where the red spectra is Keck data and the black spectra is SDSS data. For each graph, the wavelength is plotted on the x-axis between 3000 and 7000Å to contain the broad Hβ line, both [OIII] lines, and the powerlaw on the blue side of the continuum. The y-axis is individually adjusted so that the 5007Å [OIII] line is normalized to 1, see Section 2. After inspection of all 102 plots, 41/102 (40.2%) have a larger blue side emission in Keck than SDSS, 17/102 (16.7%) have more blue side emission in SDSS than Keck, and 44/102 (43.1%) show no major change.

3.1.2 Subtracted Spectra

To study the change in the broad Hβ emission line profile, the next step is to repeat this process, but for the subtracted data sets where the continuum powerlaw and stellar absorption lines are taken out. These plots for all 102 objects are shown in Appendix A.2. The x-axis range is set from 4750 to 5050Å to only show the broad Hβ and 4959Å [OIII] line. Once again the 5007Å [OIII] line is normalized to 1 and the y-axis is individually scaled for each object to better show any changes to the spectra. After inspecting

all 102 plots, 36/102 (35.3%) objects have a stronger [1] Hβ line in Keck than SDSS, 34/102 (33.3%) have a stronger broad Hβ line in SDSS than Keck, and 32/102 (31.4%) show no noticeable change.

3.1.3 Seyfert-Type Change

Typically the Hβ and Hα lines are used for Seyfert-type classification (Table 1.1), and while SDSS spectra include both lines, Keck spectra do not contain the Hα line. Thus, to determine the Seyfert-type from the Keck spectra, higher order Balmer lines (4341Å Hγ and 4102Å Hδ) were used in addition to Hβ. This is not ideal because the Hγ line is often blended together with the 4363Å [OIII] and 4383Å FeI line and the Hδ lines is always very weak, if it is even present, given the signal-to-noise ratio.

To quantify the magnitude of the Seyfert-type transitions, every transition is assigned a value between -4 and $+4$ in increments of 1. A positive value means that the object's Hβ line narrowed between SDSS and Keck while a negative value implies that the Hβ line broadened. A $+4$ value indicates a full type transition from type-1 to 2 while a value of -4 means a full transition from type-2 to 1, but is not observed in this sample. A $+3$ implies that the object transitioned three types (e.g. 1 to 1.9) while a -3 would be the opposite. A value of ± 2 indicates that the object transitioned two types (e.g. 1 to 1.8), and a ± 1 value means that the object transitioned one type (e.g. 1 to 1.5). A value of 0 indicates that the object did not experience a Seyfert-type change. Table 3.1 below provides a the Seyfert classification and time observed for SDSS and Keck, the time between observations, and the magnitude of the type transition.

Seyfert-Type Transitions

Object	I.D.	Time Taken (SDSS)	Classification (SDSS)	Time Taken (Keck)	Classification (Keck)	Time between observations years	Magnitude of Transition
0013-0951	L71	08-17-2001	1	09-20-2009	1.8	8.09	+3
0026+0009	L5	08-26-2000	1.8	09-20-2009	1.8	9.07	0
0038+0034	L73	09-06-2000	1	09-20-2009	1.8	9.04	+3
0109+0059	L74	09-07-2000	1.5	09-20-2009	1.5	9.04	0
0121-0102	L11	09-02-2000	1.5	01-21-2009	1	8.39	−1
0150+0057	L76	09-06-2000	1	09-20-2009	1	9.04	0
0206-0017	L2	09-25-2000	1	01-22-2009	1	8.33	0
0212+1406	L77	12-05-2000	1	09-20-2009	1	8.79	0
0301+0110	L78	09-30-2000	1.5	09-20-2009	1.5	8.97	0
0301+0115	L79	09-30-2000	1	09-20-2009	1	8.97	0
0310-0049	L80	12-15-2001	1	09-20-2009	1	7.76	0

Continued on next page

[1] When emission lines are being compared, the stronger emission line is broader and/or has a greater amount of flux.

Table3.1– *Continued from previous page*

Object	I.D.	Time Taken (SDSS)	Classification (SDSS)	Time Taken (Keck)	Classification (Keck)	Time between observations years	Magnitude of Transition
0336-0706	L9	12-31-2000	1.9	09-20-2009	1.9	8.72	0
0353-0623	L6	12-30-2000	1.8	01-22-2009	1	8.06	−2
0731+4522	L81	11-05-2004	1	09-20-2009	1	4.87	0
0735+3752	L82	11-29-2000	1.5	09-20-2009	1.8	8.81	+1
0737+4244	L83	01-31-2004	1.8	09-20-2009	1.5	5.64	−1
0802+3104	L1	01-02-2003	1	01-21-2009	1.5	5.97	+1
0811+1739	L114	12-18-2004	1.5	03-15-2010	1	5.24	−1
0813+4608	L10	11-29-2000	1.8	01-14-2010	1	9.13	−2
0831+0521	L208	01-07-2003	1.8	03-15-2010	1.8	7.18	0
0845+3409	L126	02-02-2003	1	03-14-2010	1	7.11	0
0846+2522	L4	12-19-2004	1.5	01-22-2009	1.5	4.09	0
0847+1842 (B)	L8	12-07-2005	1	01-21-2009	1.8	3.10	+2
0854+1741	L130	12-25-2005	1.5	03-15-2010	1	4.22	−1
0857+0528	L19	01-31-2003	1	01-15-2010	1	6.96	0
0904+5536	L20	12-30-2000	1.8	03-14-2010	1.8	9.20	0
0909+1330	L21	04-01-2006	1.8	01-14-2010	1	3.79	−2
0921+1017	L22	02-15-2004	1.9	01-14-2010	1.8	5.91	−1
0923+2254	L23	12-23-2005	1	01-15-2010	1	4.06	0
0923+2946	L138	01-19-2005	1.9	01-15-2010	1.8	4.99	−1
0927+2301	L24	12-26-2005	1.5	01-15-2010	1.5	4.05	0
0932+0233	L26	02-25-2001	1.8	01-14-2010	1.8	8.88	0
0932+0405 (B)	L27	12-21-2001	1.5	01-14-2010	1.9	8.07	+2
0936+1014	L143	12-20-2003	1.5	03-15-2010	1	6.23	−1
0938+0743 (B)	L28	04-04-2003	1	01-14-2010	1.8	6.78	+2
0948+4030	L29	03-11-2003	1	01-15-2010	1.5	6.85	+1
1002+2648	L30	01-22-2006	1.8	01-15-2010	1.9	3.98	+1
1029+1408	L155	03-11-2004	1.5	01-15-2010	1.5	5.85	0
1029+2728	L31	02-28-2006	1.8	01-15-2010	1.8	3.88	0
1029+4019	L156	01-29-2004	1.5	01-14-2010	1.5	5.96	0
1038+4658 (B)	L157	12-12-2002	1	01-14-2010	1.9	7.09	+3
1042+0414	L32	03-06-2002	1.5	04-16-2009	1.5	7.11	0
1043+1105	L33	04-20-2004	1.8	04-46-2009	1.8	4.99	0

Continued on next page

Table3.1– *Continued from previous page*

Object	I.D.	Time Taken (SDSS)	Classification (SDSS)	Time Taken (Keck)	Classification (Keck)	Time between observations years	Magnitude of Transition
1049+2451	L34	02-26-2006	1	04-16-2009	1	3.13	0
1058+5259	L162	01-13-2003	1.5	01-14-2010	1.5	7.00	0
1101+1102	L35	04-24-2004	1.5	04-16-2009	1.9	4.98	+2
1104+4334	L36	02-18-2004	1.9	01-14-2010	1.5	5.91	−2
1110+1136	L37	03-14-2004	1.5	03-15-2010	1	6.00	−1
1116+4123	L13	12-30-2003	1.8	04-15-2009	1.8	5.29	0
1118+2827 (B)	L38	02-27-2006	1.8	01-15-2010	1.9	3.88	+1
1132+1017	L14	05-22-2003	1.5	01-15-2010	1	6.65	−1
1137+4826	L39	01-03-2003	1.5	01-14-2010	1.5	7.03	0
1139+5911	L174	05-15-2002	1.5	01-14-2010	1.5	7.67	0
1140+2307 (B)	L40	05-21-2006	1.5	01-15-2010	1.9	3.66	+2
1143+5941	L177	05-17-2002	1.5	03-14-2010	1	7.82	−1
1144+3653	L15	04-16-2009	1	03-13-2005	1	4.09	0
1145+5547	L41	04-30-2003	1	03-14-2010	1	6.87	0
1147+0902	L180	05-01-2003	1.5	01-15-2010	1.5	6.71	0
1205+4959	L187	06-17-2002	1.8	01-14-2010	1.8	7.58	0
1206+4244	L42	04-25-2004	1	03-14-2010	1	5.88	0
1210+3820	L43	04-13-2005	1.5	04-16-2009	1.5	4.01	0
1216+5049	L44	05-19-2002	1.8	03-14-2010	1.8	6.82	0
1223+0240	L45	01-09-2002	1	03-15-2010	1	8.18	0
1228+0951	L210	04-02-2003	1.9	03-15-2010	1.9	6.95	0
1231+4504	L196	02-27-2004	1.5	01-15-2010	1.5	5.88	0
1241+3722	L197	04-02-2006	1.5	01-15-2010	1.5	3.79	0
1246+5134	L202	04-15-2002	1.9	01-15-2010	1.8	7.75	−1
1250-0249	L46	03-29-2001	1.5	04-16-2009	1.8	8.05	+1
1306+4552	L47	04-22-2004	1	03-14-2010	1.5	5.89	+1
1307+0952	L48	05-29-2006	1.8	03-15-2010	1.5	3.79	−1
1312+2628	L204	02-28-2006	1.5	03-14-2010	1	4.04	−1
1313+3653	L213	03-21-2006	1.8	03-14-2010	1.8	3.98	0
1323+2701	L49	03-01-2006	1.8	04-16-2009	1.8	3.13	0
1353+3951 (B)	L207	02-26-2004	1.5	03-14-2010	2	6.05	+2
1355+3834	L50	03-31-2005	1.9	04-16-2009	1.9	4.04	0

Continued on next page

Table3.1– *Continued from previous page*

Object	I.D.	Time Taken (SDSS)	Classification (SDSS)	Time Taken (Keck)	Classification (Keck)	Time between observations years	Magnitude of Transition
1405-0259	L51	06-18-2002	1	04-16-2009	1.5	6.83	+1
1416+0317	L52	03-26-2001	1.5	03-15-2010	1.8	8.97	+1
1419+0754	L53	06-12-2005	1.8	04-16-2009	1.8	3.84	0
1423+2720 (B)	L209	05-26-2006	1.5	03-14-2010	1.9	3.80	+2
1434+4839	L54	04-04-2003	1	04-16-2009	1.5	6.03	+1
1505+0342	L56	05-26-2001	1.8	03-15-2010	1.5	8.80	−1
1535+5754	L57	03-14-2002	1	04-15-2009	1	7.09	0
1543+3631	L214	08-24-2003	1	03-15-2010	1.5	6.56	+1
1545+1709	L58	06-03-2006	1.8	04-15-2009	1	2.87	−2
1554+3238	L59	07-05-2003	1.5	04-15-2009	1.5	5.78	0
1557+0830	L60	08-11-2004	1.5	04-15-2009	1.5	4.68	0
1605+3305	L61	05-17-2004	1	04-15-2009	1	4.91	0
1606+3324	L62	05-19-2004	1.9	04-15-2009	1.8	4.91	−1
1611+5211	L63	05-22-2001	1.5	04-15-2009	1.9	7.95	+2
1636+4202	L205	06-23-2001	1	03-14-2010	1	8.72	0
1647+4442	L64	05-22-2001	1.9	03-14-2010	1.8	8.81	−1
1655+2014	L88	06-13-2004	1.8	09-20-2009	1.8	5.27	0
1708+2153	L91	06-21-2004	1.5	09-20-2009	1	5.25	−1
2116+1102	L96	07-13-2002	1.8	09-20-2009	1.8	7.19	0
2140+0025	L99	07-10-2002	1	09-20-2009	1	7.20	0
2215-0036	L100	09-04-2000	1	09-20-2009	1	9.04	0
2221-0906	L102	10-21-2001	1	09-20-2009	1	7.92	0
2222-0819	L103	10-24-2001	1.5	09-20-2009	1.5	7.91	0
2233+1312	L106	09-04-2002	1	09-20-2009	1.5	7.04	+1
2254+0046	L108	09-02-2000	1	09-20-2009	1	9.05	0
2327+1524	L70	11-25-2001	1.8	09-20-2009	1.9	7.82	+1
2351+1552	L109	11-13-2001	1.9	09-20-2009	1.9	7.85	0

Table 3.1: SDSS and Keck Seyfert-type classifications for all 102 objects in the sample. Objects from Scott et al. (2012) are marked with a "B". The average time between observations is 6.44 ± 1.84 years.

To count the number of occurrences for each magnitude of Seyfert-type transition, a histogram is provided below in Figure 3.1.

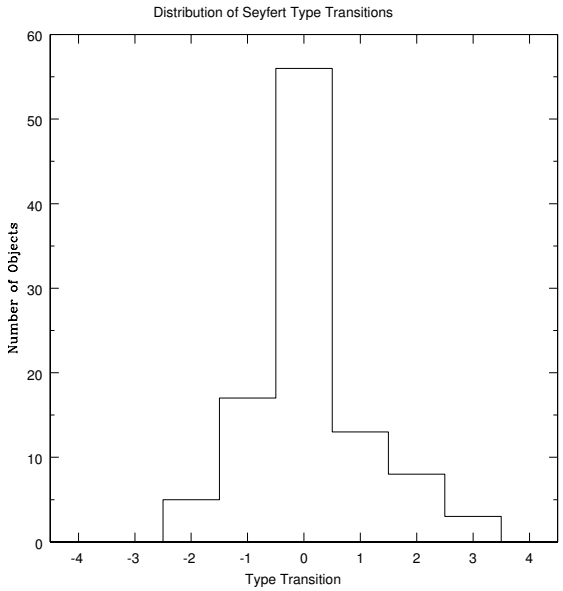

Figure 3.1: Magnitude of Seyfert-type transitions.

Figure 3.1 and Table 3.1 show that while the majority of the objects in our sample do not experience a type transition, 45/102 (44%) do change type. It can also be seen that the there is more change towards narrower lines in Keck, indicated by the larger number of positive values in Table 3.1. For a comparison of time between observations and magnitude of Seyfert-type change, see Figure 3.2 below.

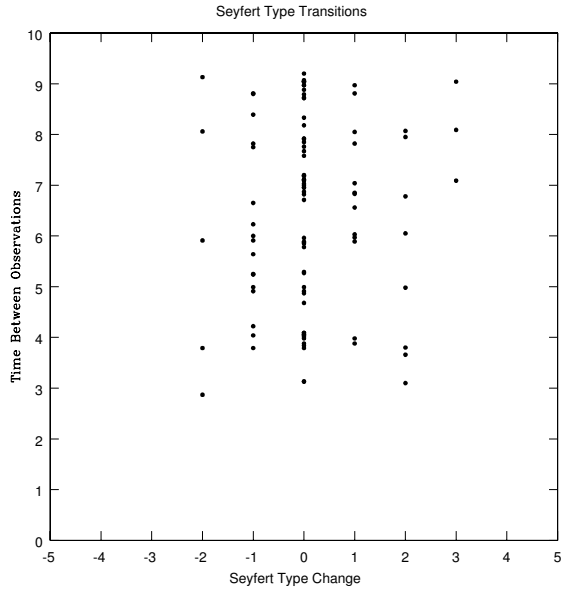

Figure 3.2: Time between observations vs. magnitude of Seyfert-type change.

Figure 3.2 shows that there is no trend between time elapsed and amount of Seyfert-type change,

indicating that the type change may happen on shorter time scales than those covered.

3.2 Quantitative Analysis

3.2.1 Hβ Fitting

While in the previous section, the relative strengths of the powerlaw and Hβ line were compared visually, the Hβ line can be fitted to compare the flux and width quantitatively. For this, the narrow component of the Hβ line is fitted with a single Gaussian and the broad Hβ and both [OIII] lines (4959Å and 5007Å) are fitted using a combination of Gauss-Hermite polynomials. Gaussian fits are symmetric; however, emission lines are known to be asymmetric. Hermite polynomials are used as an extension of the Gaussian fit to account for these asymmetries (Weisstein 2015). Gauss-Hermite polynomials can be used to fit the broad Hβ and both [OIII] lines by centering a Gauss-Hermite function at the peak of each emission line. A Gauss-Hermite polynomial of the order 2-5 was used to fit the broad Hβ line while a polynomial of the order 2-12 was used to fit the [OIII] lines. The subtracted data sets are used for fitting because the underlying absorption spectrum is gone, giving a more accurate evaluation of the Hβ line. For this part, the sample is cut down to 79 objects included in Bennert et al. (2015) for which this analysis was done on the Keck spectra by Dr. Vardha N. Bennert & Rebecca Rosen. The plots of the SDSS and Keck Hβ and [OIII] fits as derived in this thesis are shown in Appendix B. The x-axis again ranges between 4750 and 5050Å and the y-axis is manually adjusted for each object to better show the broad Hβ and the first [OIII] lines, note that the two [OIII] lines are in a flux ratio of 1:3. When looking at these plots the black line is the data, the red line is the fit to the data, the green line is the broad Hβ fit, and the blue line is the residual. Seven different values are obtained from this fitting method:

1. The second moment of the model to the broad Hβ line ($\sigma_{\mathrm{H}\beta}$). This is the velocity dispersion of the broad Hβ line derived from the model. This is the measurement of the Hβ width used in estimating M_{BH}

2. The full width at half maximum (FWHM) of the Hβ line. For a Gaussian profile, FWHM = $2.35\sigma_{\mathrm{H}\beta}$.

3. The logarithmic $M_{BH}/M_{\odot}$. The formula used to calculate M_{BH} is derived from the most recent BLR radius-luminosity relation (Bentz et al. 2013) where $\log(f) = 0.71$:

$$\log(M_{BH}/M_{\odot}) = 0.71 + 6.849 + 2\log(\frac{\sigma_{H\beta}}{1000\mathrm{km\ s^{-1}}}) + 0.549\log(\frac{L_{5100}}{10^{44}\mathrm{erg\ s^{-1}}}) \tag{3.2.1}$$

   Here L_{5100} is the continuum luminosity at 5100Å determined from SDSS g' band surface photometry (Bennert et al. 2015).

4. The second moment of the data to the broad Hβ line. This is the velocity dispersion of the broad Hβ line derived from the data.

5. The ratio of flux between the narrow Hβ line and [OIII] lines, Hβ/[OIII].

6. The ratio of flux between the narrow Hβ component and broad Hβ component, Hβ_{narrow}/Hβ_{broad}.

Separate plots for each different values can be seen in Figures 3.3 - 3.8 below. On all six graphs, SDSS data is plotted on the y-axis, Keck data is on the x-axis, and a unity line is included for better comparison. The farther from this unity line the data points deviate, the more that object has changed between the data sets. A chart including the average ratio and scatter of the data for each of these six graphs is also provided below. An average above one will indicate that most objects were stronger in SDSS than Keck, while an average below one will indicate the opposite. The scatter indicates how far data points deviate from the average value.

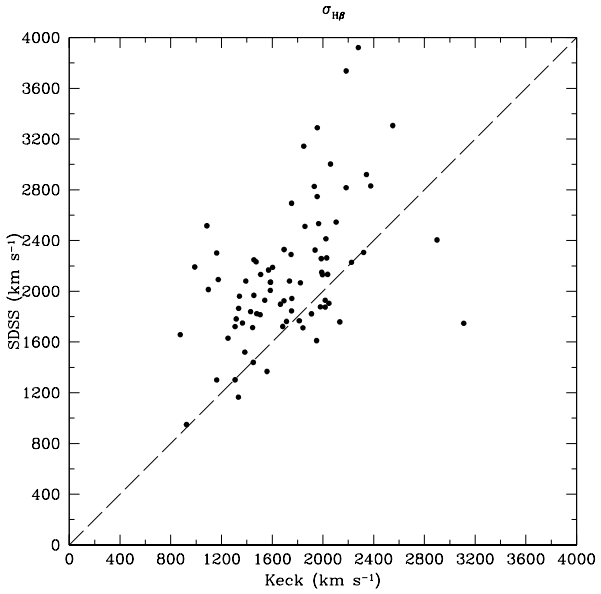

Figure 3.3: Second moment of the model to the broad Hβ line SDSS vs. Keck. The dashed line is the unity line.

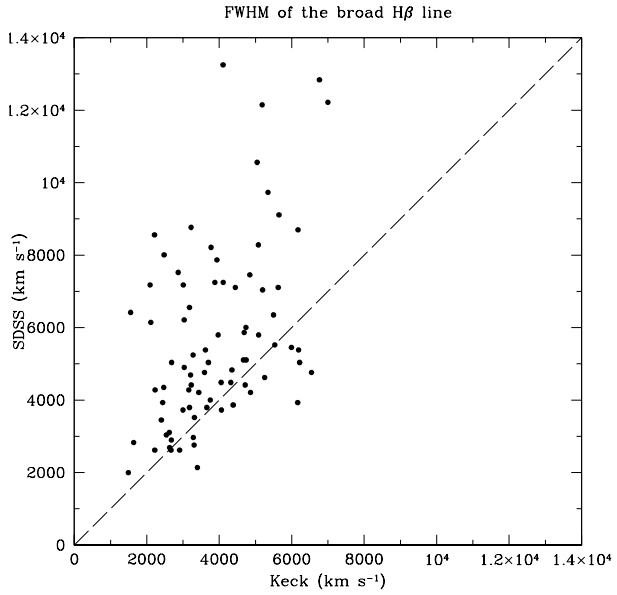

Figure 3.4: FWHM SDSS vs. Keck. The dashed line is the unity line.

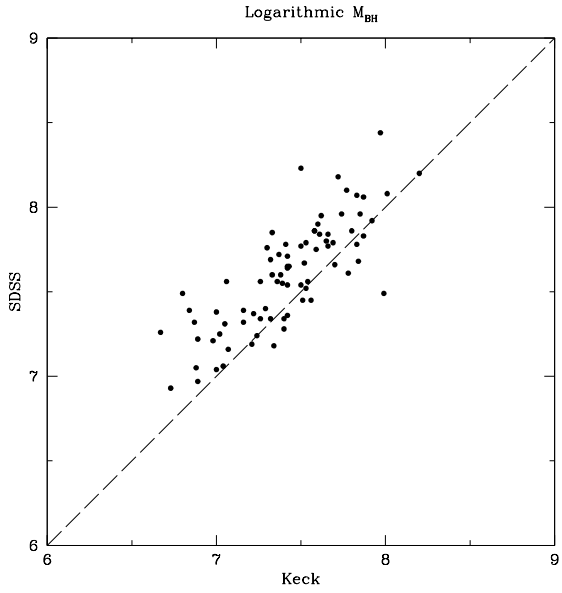

Figure 3.5: Logarithmic M_{BH} SDSS vs. Keck in units of $M_{\odot}$. The dashed line is the unity line.

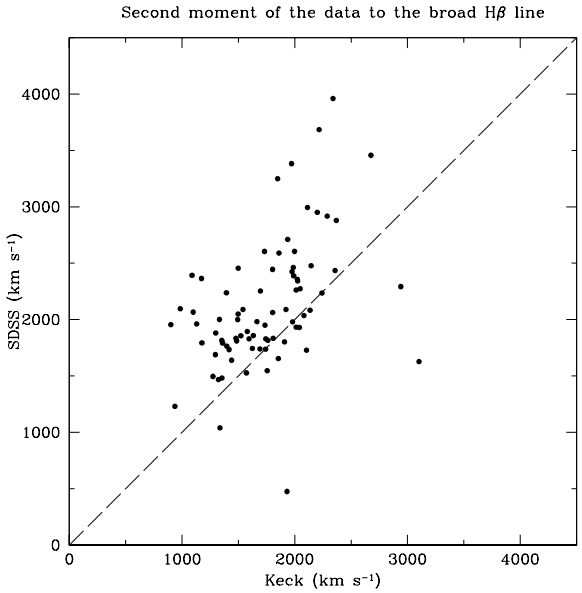

Figure 3.6: Second moment of the data to the broad Hβ line SDSS vs. Keck. The dashed line is the unity line.

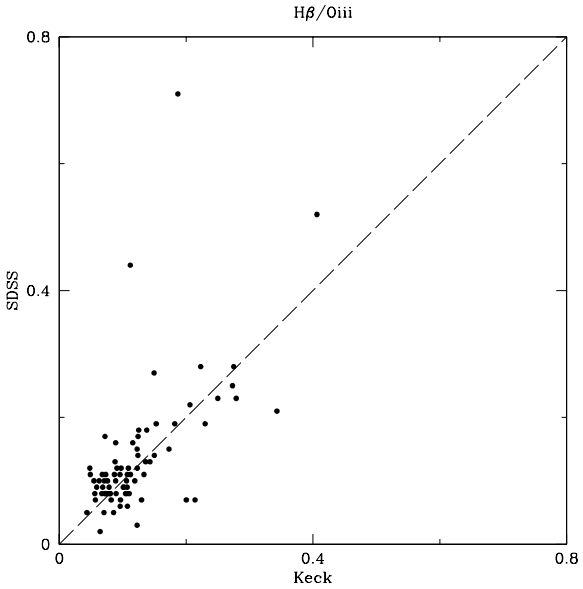

Figure 3.7: The flux ratio between the narrow Hβ line and [OIII] lines. Note that one outlier was omitted from the plot to better show the rest of the data. This object, 2140+0025, is the only object in the sample where the Hβ line is stronger than the [OIII] lines, thus causing the flux ratio to be greater than 1. The dashed line is the unity line.

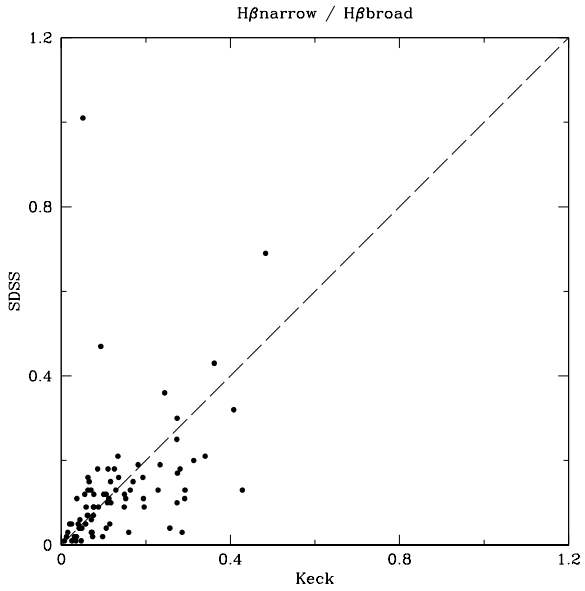

Figure 3.8: The flux ratio between the narrow Hβ line and broad Hβ line. The dashed line is the unity line.

Broad Hβ Fitting Statistics		
Data	Average	Scatter
$\sigma_{\mathrm{H}\beta}$	1.26	0.31
FWHM	1.54	0.72
$\mathrm{Log}(M_{\mathrm{BH}}/M_{\odot})$	1.02	0.03
Second moment of the data of broad Hβ	1.25	0.34
Hβ/[OIII] ratio	1.17	0.61
$\mathrm{H}\beta_{\mathrm{narrow}}/\mathrm{H}\beta_{\mathrm{broad}}$	1.31	2.24

Table 3.2: Average and scatter for broad Hβ fitting methods. (Figures 3.3-3.8)

The averages from Figures 3.3, 3.7, and 3.8 indicate that the Hβ line is generally stronger in SDSS than Keck. $\sigma_{\mathrm{H}\beta}$ is 26% larger in SDSS spectra than Keck, causing SDSS $\log(M_{\mathrm{BH}}/M_{\odot})$ to be greater by 2%. The average and scatter for $\sigma_{\mathrm{H}\beta}$ and the second moment of the data of broad Hβ are very close indicating that our model accurately represents the data. From the averages of Figures 3.3 and 3.4, FWHM $\neq 2.35\sigma_{\mathrm{H}\beta}$ (as would be the case for a Gaussian) due to the asymmetries in the broad Hβ line.

3.2.2 Continuum Powerlaw

Changes to the continuum powerlaw are also quantified in more detail. The powerlaw was calculated for all unsubtracted Keck and SDSS files using a $y = Ax^b$ equation where A is a scaling factor and b is an exponent of x and both can vary in value. The value of the exponent is important because it controls the shape of the powerlaw. The values for b for SDSS and Keck are in Appendix C. The purpose of finding b is to test to see if either one is a potential driving force to the observed change in the Hβ line. This could be a possibility because the powerlaw comes from the accretion disk and ionizes the broad Hβ line. To accomplish this, we will compare the exponent with $\sigma_{\mathrm{H}\beta}$. The ratio of SDSS and Keck $\sigma_{\mathrm{H}\beta}$ vs. the ratio of SDSS and Keck powerlaw exponent, b, (Figure 3.9). A unity line was added to make comparisons easier. Also below is a table of statistics showing the average and scatter of Figure 3.9.

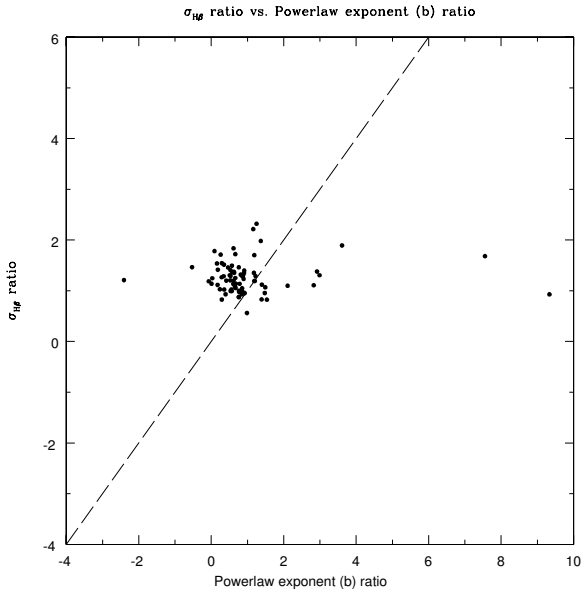

Figure 3.9: SDSS/Keck $\sigma_{\mathrm{H}\beta}$ ratio vs. SDSS/Keck exponent ratio. The dashed line is the unity line.

Continuum Powerlaw Fitting Statistics		
Data	Ratio	Scatter
$\sigma_{\mathrm{H}\beta}$ vs. powerlaw exponent	3.97	14.31

Table 3.3: Average and scatter for continuum powerlaw exponent. (Figure 3.9)

From Figure 3.9 there is no clear correlation between the changes in the width of the broad Hβ line and continuum powerlaw. This is supported by the large scatter.

3.2.3 Hβ Line Flux Variations

From Figures 3.3, 3.7, and 3.8 it is clear that the Hβ line changed shape and its flux ratio with the [OIII] line. Figure 3.10 below tests if changes in Hβ flux correlate with changes to $\sigma_{\mathrm{H}\beta}$. The average and scatter for Figure 3.10 are included in Table 3.4.

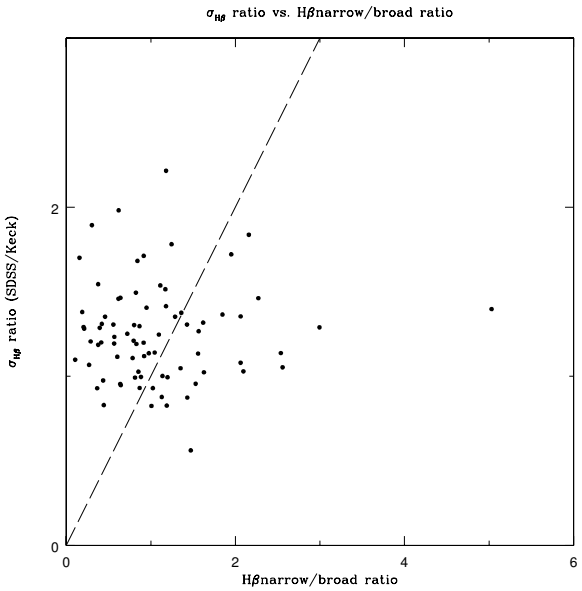

Figure 3.10: $\sigma_{\mathrm{H}\beta}$ ratio SDSS/Keck vs. $\mathrm{H}\beta_{\mathrm{narrow}}/\mathrm{H}\beta_{\mathrm{broad}}$ ratio SDSS/Keck. The dashed line is the unity line.

$\sigma_{\mathrm{H}\beta}$ vs. $\mathrm{H}\beta_{\mathrm{narrow}}/\mathrm{H}\beta_{\mathrm{broad}}$ Statistics		
Data	Ratio	Scatter
$\sigma_{\mathrm{H}\beta}$ vs. powerlaw exponent	1.32	0.83

Table 3.4: Average and scatter for continuum powerlaw exponent. (Figure 3.10)

It is clear from Figure 3.10 that variations to the width and flux of the Hβ line do not correlate with any of the probed quantities. To test if changes to the continuum are the driving force responsible for this observed change in Hβ line shape, two plots are shown below, all axes are SDSS/Keck:

1. Powerlaw exponent ratio vs. Hβ/[OIII] ratio
2. Powerlaw exponent ratio vs. $\mathrm{H}\beta_{\mathrm{narrow}}/\mathrm{H}\beta_{\mathrm{broad}}$

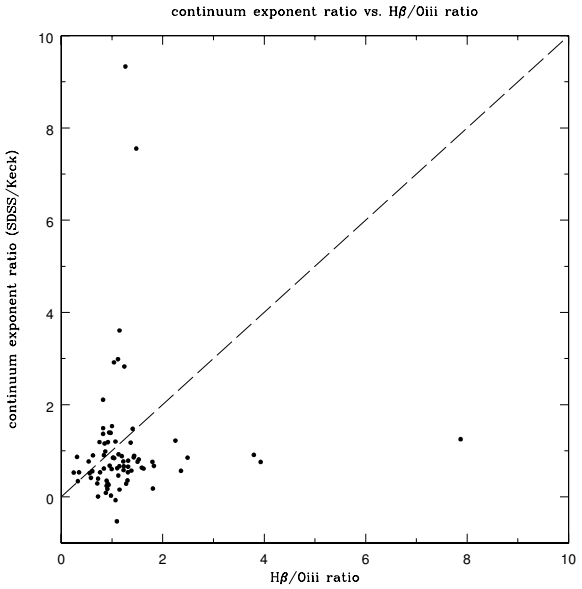

Figure 3.11: Powerlaw exponent ratio SDSS/Keck vs. Hβ/[OIII] ratio SDSS/Keck. The dashed line is the unity line.

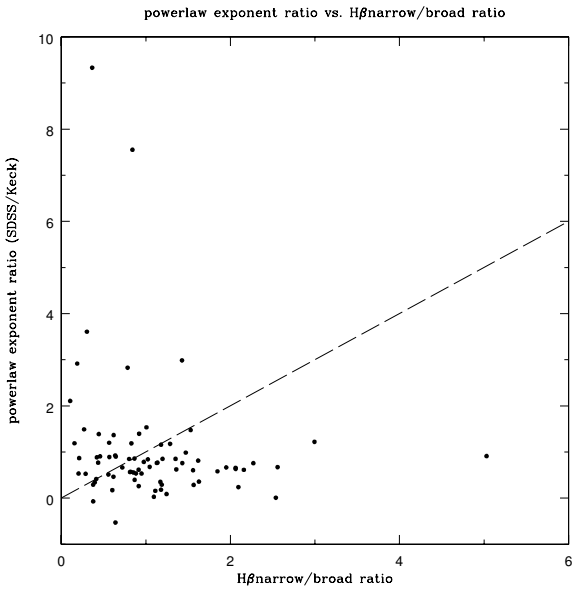

Figure 3.12: Powerlaw exponent ratio SDSS/Keck vs. H$\beta_{\rm narrow}$/H$\beta_{\rm broad}$ SDSS/Keck. The dashed line is the unity line.

Powerlaw vs. Hβ flux statistics		
Data	Average	Scatter
Powerlaw exponent ratio vs. Hβ/[OIII] ratio	0.94	1.18
Powerlaw exponent ratio vs. Hβ_{narrow}/Hβ_{broad}	1.95	4.27

Table 3.5: Average and scatter for continuum powerlaw vs. Hβ flux comparison. (Figures 3.11-3.12)

It is clear from Figures 3.11 and 3.12 that changes to the continuum powerlaw do not correlate to the observed Hβ line change, and Chapter 4 will explore other possible reasons for this change.

3.2.4 FeII Emission Line Subtraction

For 55 objects, FeII emission lines were subtracted from the Keck spectra, but not from the correlating SDSS spectra, due to insufficient signal-to-noise ratio and resolution of the latter. To test if this introduces a bias, Figures 3.3 and 3.9 are re-made, and objects that are FeII subtracted are the black data points while green data points represent objects containing FeII lines. These two graphs are Figures 3.13 and 3.14 below with an accompanying chart of average and scatter statistics.

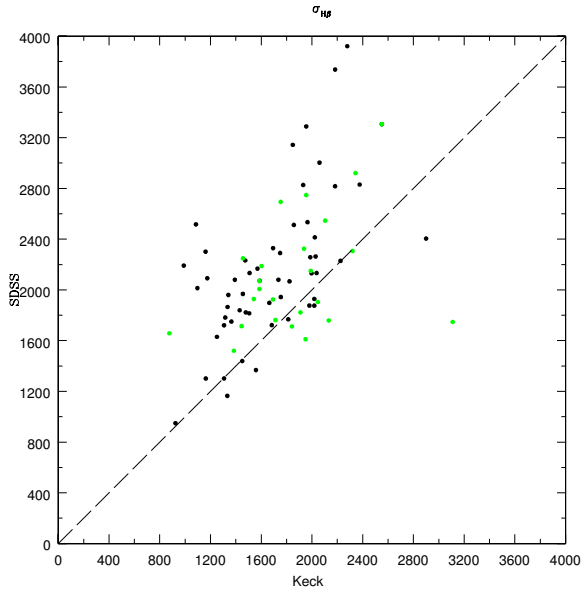

Figure 3.13: Same plot as Figure 3.3 but objects that had FeII lines subtracted are black and green points did not. The dashed line is the unity line.

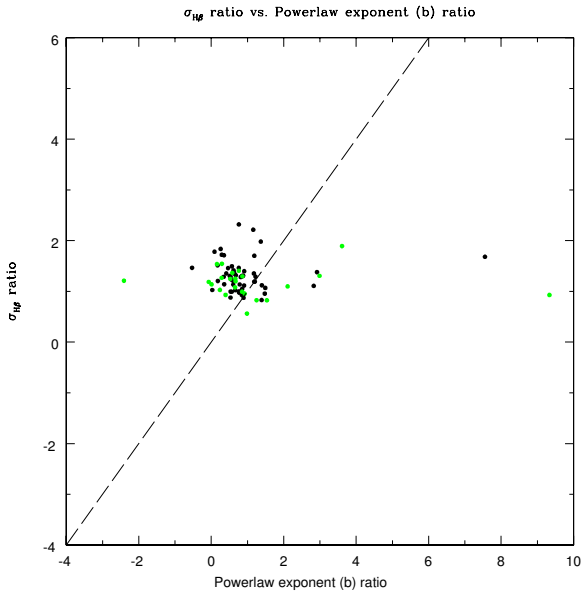

Figure 3.14: Same plot as Figure 3.9 but objects that had FeII lines subtracted are black and green points did not. The dashed line is the unity line.

FeII subtraction statistics			
Plot	FeII subtracted	Average	Scatter
$\sigma_{\mathrm{H}\beta}$ SDSS vs. Keck	Yes	1.31	0.32
$\sigma_{\mathrm{H}\beta}$ SDSS vs. Keck	No	1.17	0.28
$\sigma_{\mathrm{H}\beta}$ vs. powerlaw exponent	Yes	2.99	5.51
$\sigma_{\mathrm{H}\beta}$ vs. powerlaw exponent	No	6.09	24.34

Table 3.6: Average and scatter for FeII subtraction comparison. (Figures 3.13-3.14)

The slightly higher average in $\sigma_{\mathrm{H}\beta}$ of SDSS vs. Keck (1.31 $\pm$ 0.32 and 1.17 $\pm$ 0.28) indicates that not subtracting the FeII line in SDSS spectra can potentially atrificially broaden the Hβ line. However, given the large scatter, the bias is not significant and cannot explain the change in Hβ line observed. Note that Maren Cosens is currently in the process of using an updated code to analyze the Keck and SDSS spectra in a homogeneous way, to rule out the effect of FeII completely.

Chapter 4

Discussion of Results

4.1 Seyfert-Type Change in the Sample

A Seyfert-type change is not predicted within the unified model in which the type solely depends on viewing angle. However, 45/102 (44%) of the objects in our sample experience a type transition within approximately a 3-9 year time span (Table 3.1). The majority of the objects that experience a type change transition toward narrower lines in Keck data, which might simply be a reflection of our selection bias. The observed change in Seyfert-type calls for a modification to the simple unified model with Seyfert-type depending only on viewing angle. The two typically accepted causes for Seyfert-type transitions are either variable obscuration (e.g. dusty torus) or variable accretion rate (Denney et al. 2014). Variable accretion rates cause the amount of light given off by accretion disc to change which in turn alters the strength of the continuum. Since the continuum powerlaw is responsible for ionizing the BLR, the Hβ line flux can change. Variable obscuration is mainly due to the irregular ring of individual gas and dust clouds that makes up the dusty torus surrounding the BLR. Individual dust clouds can pass in front of the BLR and more light at certain times.

4.2 Observations from the Data

One notable observation from Figures 3.3 - 3.8 is that more points lie above the unity line indicating that SDSS Hβ lines are broader than their Keck counterparts on average. This is likely due to the initial sample selection, as only SDSS objects with a broad Hβ line were selected to be remeasured by Keck. This introduces a bias as our sample contains no SDSS objects with only a narrow Hβ line. The large variability of the broad Hβ line in many objects questions the ability to estimate $M_{\rm BH}$ for the single epoch method. However, it is known from reverberation mapping that the flux of the broad Hβ line changes in response to continuum changes in a way that the resulting $M_{\rm BH}$ is conserved. Also, in our data, the resulting change in $M_{\rm BH}$ is small (1.02 ± 0.03), especially when taking into account the large uncertainty involved when measuring $M_{\rm BH}$ (0.4 dex).

Figure 3.7 implies that either the narrow Hβ component or the [OIII] lines have changed flux between SDSS and Keck measurements, bringing into question the validity of the [OIII] scaling stated earlier in this thesis. Both lines originate from the narrow line region, which is not expected to change over this time scale. One possibility is that the fit to the broad Hβ component also changed the fit to the narrow component, since both lines are blended and it is difficult to disentangle them, especially when the broad Hβ component is dominant. However, such an effect is likely to be small and the observed scatter in Figure 3.8 instead questions the scaling to a constant [OIII] line. However, while a change in flux in the narrow lines based on different regions covered in the SDSS vs. Keck spectra could result in an artificial change in broad Hβ flux (if scaled on [OIII]), it cannot explain a change in the profile of Hβ. So objects for which the broad Hβ emission line profile changes are good candidates for a real change in the BLR.

Figures 3.9, 3.11, and 3.12 show that variable accretion cannot be the only force for most objects in our sample, because the powerlaw is not the major driving force behind the observed changes to the Hβ line. The few objects that lie on the unity line in Figures 3.11 and 3.12 are the more likely candidates for variable accretion because the changes to powerlaw and Hβ flux is equivalent. Figure 3.10 shows that variable obscuration also cannot be the only force for the majority of the objects in our sample because there is not correlation between changes to the broad Hβ width and flux. A scenario in which variations in both accretion and obscuration drive the change in the broad Hβ line is a possibility. Without further information, it cannot be determined which factor caused changes to the broad Hβ line for each individual object. Objects with a weaker Hβ line in Keck could be explained by a more opaque torus or dust clouds in the line of sight or less accretion at the time of observation, while objects with broad Hβ line growth are due to either a less opaque torus/dust clouds or more accretion during observation. To ultimately determine the cause of the observed broad Hβ line variability, more observations and tests are necessary. One approach is to look for existing archival/literature data, also at other wavelengths (e.g. X-rays and UV) that could shed light on the origin (see comparison to literature below.) Follow-up observations are another approach. Both are beyond the scope of this thesis.

4.3 Comparison to Literature

4.3.1 Comparison to Scott et al.

As mentioned in Section 1.3, Bryan Scott inspected eight objects from the sample where the broad component of the Hβ line is very small or non-existent in Keck. These objects are marked with a "B" in Table 3.1. All eight objects transitioned to either type-1.8, 1.9, or 2 when remeasured at Keck. Here is an abbreviated list of possible explanations for the observed drastic change outlined by Scott:

1. Supernova: A supernova gives off many broad lines including Balmer lines, so AGN and supernova spectra are very similar. In this scenario, the object is a supernova in the center of an inactive galaxy that was mistaken for an AGN in the SDSS spectrum. The supernova has faded since, and the broad lines have disappeared in the Keck spectra.

2. Galaxy merger: An AGN offset from the center of its host galaxy could result from a merger between an active and an inactive galaxy. In this scenario, the wider SDSS spectrum included the AGN, while the narrower Keck spectrum missed the offset AGN as it was pointed on the center of the galaxy. This could be determined by imaging the object to look for visible signs of a merger.

3. Gravitational recoil of supermassive BHs: A merger of two BHs at the center of the AGN would cause the two BHs to orbit each other producing gravitational waves that are analogous to electromagnetic waves emitted by an accelerated charged particle. The final merger of the two BHs can lead to a so-called gravitational recoil, with the resulting BH being kicked out of the center of the center of the galaxy, carrying the BLR with it. This scenario is similar to the AGN offset mentioned above as it could be the reason for such an offset, and again, the AGN was missed in the Keck spectra.

While these three possibilities could explain an observed apparent Seyfert-type change for individual objects, none of these are viable options to explain the observed change for the entire sample, simply because they are too rare of a phenomenon. In any case, more data is needed to test these scenarios.

4.3.2 Comparison to Other Literature

There are many studies that report a Seyfert-type change. However, most papers only discuss one or two objects, while this thesis contains a statistically significant sample size. Variable accretion rates is cited more frequently in the literature than variable obscuration. Shappee et al. (2014) and Trippe et al. (2008) observed NGC 2617 transition from type-1.8 to type-1 and NGC 2992 transition from type-2 to type-1.5 respectively. Both papers report that an increase in X-ray flux that was followed by a boost of flux in the UV-NIR (near IR) regime causing broader emission lines. Note that it is the UV/optical emission that causes the ionization of the hydrogen gas in the BLR. Denney et al. (2014) witnessed NGC 863 over a 40 year time period transition from Seyfert-1.5 to Seyfert-1 then to Seyfert-2 and attribute this to an increase in luminosity from more accretion followed by a larger decrease in luminosity from less accretion. UV/optical and X-ray flux are observed to increase and decrease simultaneously. On long timescales, variations of the accretion disk can lead to X-ray variability and UV/optical changes (Czerny 2006).

Unlike variable accretion, X-ray flux does not vary with optical/UV in variable obscuration; this is a key way to tell the difference between the two (Denney et al. 2014). Change to the dusty torus is cited to explain variable obscuration; however, there could be other sources of dust outside of the AGN contributing as well, e.g. dust in the spiral arms of a galaxy. However, changes on timescales of the observed order of 3-9 years are not expected for dust further out in the galaxy. Currently, we do not have information about the X-ray variability in our sample. We will look into existing archival data; however, this is beyond the scope of this thesis.

Finally, another possibility for observing a Seyfert type-1 to type-2 transition is that the accretion rate is slowing down, leading to the final stages of life for an AGN and the galaxy is "turning off". However,

this is a rare event, especially at low redshifts (Denney et al. 2014), so it cannot explain the observed changes for all objects in our sample.

Chapter 5

Conclusions

This thesis utilizes a sample of ∼100 local ($0.02 \leq z \leq 0.1$) AGNs with black hole masses $M_{\rm BH} > 10^7 M_{\odot}$, selected from SDSS, and re-measured using the Keck 10-m telescope. The main purpose of the sample is to study the local scaling relations between $M_{\rm BH}$ and the host galaxy properties (see Bennert et al. 2011; 2015); however, as a side product, the data provides insight into any changes of the broad-line region within the 3-9 year time-frame covered by the two sets of spectra. After standard reduction steps, the Hβ line was visually compared between the two sample. The width and strength of the Hβ line varied in approximately 66% of the objects in our sample, enough to change the Seyfert-type classification in 44% of them. The Hβ line in most objects became weaker between SDSS and Keck observations by an average of 1.26 and scatter of 0.31, but this can be attributed to sample selection as no objects with a narrow Hβ line were originally selected from SDSS. The 5007Å [OIII] line is scaled to 1 when comparing the SDSS and Keck spectra, because it originates from the NLR which is not expected to vary over the observed timescales. It is not clear that this assumption is always valid. However, it would only affect the flux, not the line profile, but most of the objects display a change in line profile as well as flux, pointing toward a real change in the broad Hβ line.

The two most likely explanations for Seyfert-type change cited in the literature are variable accretion and variable obscuration. This is an extension to the standard unified model in which Seyfert-type is solely due to the viewing angle. This suggests that while the unified model is not wrong, it could be incomplete and needs to be modified to better explain the observed Seyfert-type transitions. To test these two possibilities, the broad Hβ and both [OIII] lines were fitted using a combination of Gauss-Hermite polynomials to derive the width of the broad Hβ line. Also, the AGN powerlaw continuum was fitted as a powerlaw. Our analysis shows that the origin of the observed Hβ line change cannot be a variation in accretion (as traced by the continuum powerlaw) or obscuration (as traced by the change in narrow-to-broad Hβ flux) alone; however, a combination of both cannot be ruled out. X-ray emission, thought to drive UV/optical emission that ionized the hydrogen in the BLR, could shed light on variable accretion, but we do not currently have x-ray observations for the sample. Other possible explanations for the observed (apparent) variations to the broad Hβ line include supernova, galaxy mergers, and gravitational

recoil for supermassive BHs; however, these are rare events.

The next step is to collect more information on these objects, either from archival/literature data or follow-up observations to test different scenarios. The advantage of our sample is its size that allows a statistically meaningful assesment of the frequency of Seyfert-type changes in active galaxies and thus foster our understanding of AGNs and the unified model.

Chapter 6

Acknowledgements

I would like to thank Dr. Vardha N. Bennert for helping me grow as a physicist and preparing me for graduate school and beyond; I would not be the scientist that I am today without her guidance. I would also like to thank Bryan Scott whose work provided an excellent launching point for my research. I would like to thank Dr. Matthew Auger who wrote the Python scripts used to preform the Hβ line and continuum fitting and provided help throughout this thesis. I would like to thank Dr. Stefanie Komossa for help and guidance in the project. Assistance from a National Science Foundation (NSF) Research at Undergraduate Institutions (RUI) grant AST-1312296 is gratefully acknowledged. Note that findings and conclusions do not necessarily represent views of the NSF. This research has made use of the Dirac computer cluster at Cal Poly, maintained by Dr. Brian Granger and Dr. Ashley Ringer McDonald. Data presented in this thesis were obtained at the W. M. Keck Observatory, which is operated as a scientific partnership among Caltech, the University of California, and NASA. The Observatory was made possible by the generous financial support of the W. M. Keck Foundation. The authors recognize and acknowledge the very significant cultural role and reverence that the summit of Mauna Kea has always had within the indigenous Hawaiian community. We are most fortunate to have the opportunity to conduct observations from this mountain. This research has made use of the public archive of the Sloan Digital Sky Survey (SDSS) and the NASA/IPAC Extragalactic Database (NED) which is operated by the Jet Propulsion Laboratory, California Institute of Technology, under contract with the National Aeronautics and Space Administration. Funding for travel to Lick observatory was provided through the College Based Fee (CBF) and the Physics department at Cal Poly.

Bibliography

Bennert, et al. 2011, ApJ, 726, 59

Bennert et al. 2015; ApJ submitted (arXiv 1409.4428)

Bentz, M.C. et al. 2007, ApJ, 662, 205

Bentz, M.C. et al. 2006, ApJ, 651, 775

Bentz, M.C. et al. 2013, ApJ, 767, 149

Brewer, B.J. et al. 2011, ApJ, 733, L33

Czerny & Bozena. 2006, ASP, Vol. 360

Denney, K.D. et al. 2014, ApJ, 796, 134

Ferrarese, L., & Merritt, D. 2000, ApJ, 539, L9

Gebhardt, K., et al. 2000, ApJ, 539, L13

Kaspi, S. et al. 2005, ApJ, 629, 61

Kaspi, S. et al. 2000, ApJ, 533, 631

Kormendy, J., & Richstone, D. 1995, ARA&A, 33, 581

"LRIS: Home Page." *Keck Observatory*. 2014. http://www2.keck.hawaii.edu/inst/lris/

Magorrian, J., et al. 1998, ApJS, 117, 25

Morgan, Siobahn. "Distant and Weird Galaxies." 2002.
http://www.uni.edu/morgans/astro/course/Notes/section3/new13.html

Osterbrock, D.E. 1977, ApJ, 215, 733.

Osterbrock, D.E. 1981, ApJ, 249, 462.

Pancoast, A. et al. 2011, ApJ, 730, 139

Pancoast, A., et al. 2012, ApJ, 754, 49

Pancoast, A. et al. 2014, ApJ, submitted (arXiv:1311.6475)

Peterson, B.M. *An Introduction to Active Galactic Nuclei*. (Cambridge University Press, Cambridge, UK 2003)

Rosen, R et al. *Orbital Velocities in the Broad Line Region of Seyfert 1 Galaxies*. Cal Poly Digital Commons. 2012.

Shappee, B.J. et al. 2014, ApJ, 788, 48

Scott, B. et al. *Time Variation of the Broad Hβ and Hα Emission Lines in Active Galactic Nuclei*. Cal Poly Digital Commons. 2013.

"Survey Instruments." *SDSS Data Release 6*. 2003.

http://classic.sdss.org/dr6/instruments/index.html

Trippe, M.L. et al. 2008, ApJ, 135, 2048

Wandel, A. et al. 1999, ApJ, 526, 579

Weisstein, Eric W. "Hermite-Gauss Quadrature." From MathWorld–A Wolfram Web Resource. 2015. http://mathworld.wolfram.com/Hermite-GaussQuadrature.html

Appendix A

Qualitative Analysis Plots

A.1 Unsubtracted Spectra

This section overlays the unsubtracted SDSS and Keck spectra for every object in our sample to compare changes to the continuum between 3000-7000Å.

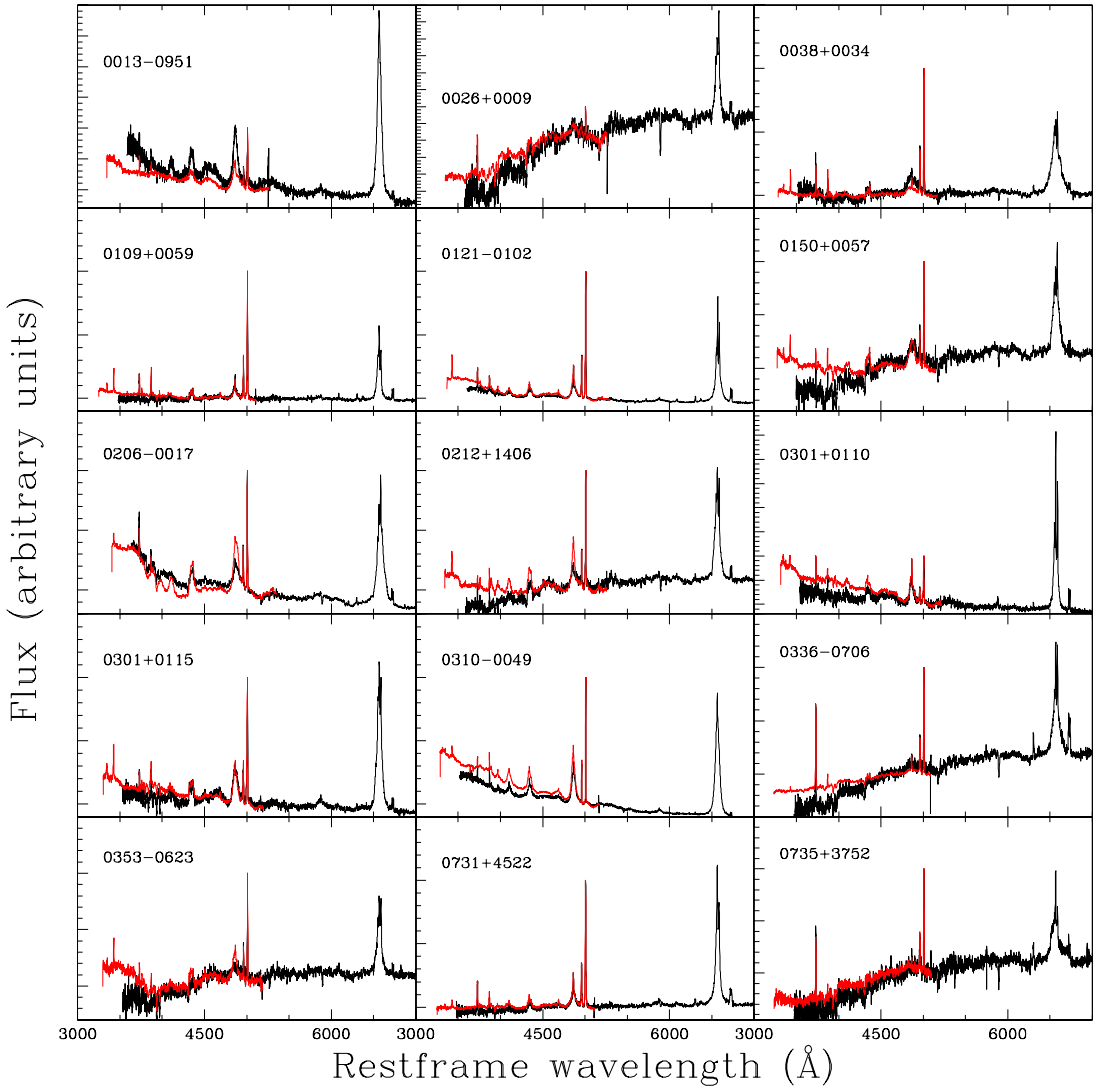

Figure A.1: 15 objects from the unsubtracted data. The black spectra is SDSS and the red spectra is Keck. A wide range of the continuum (3000-7000Å) is shown here to compare how it changes between the two sets of data. To make the data sets comparable, the base of the [OIII] line was set to 0 and the peak at 1 as disussed in the text.

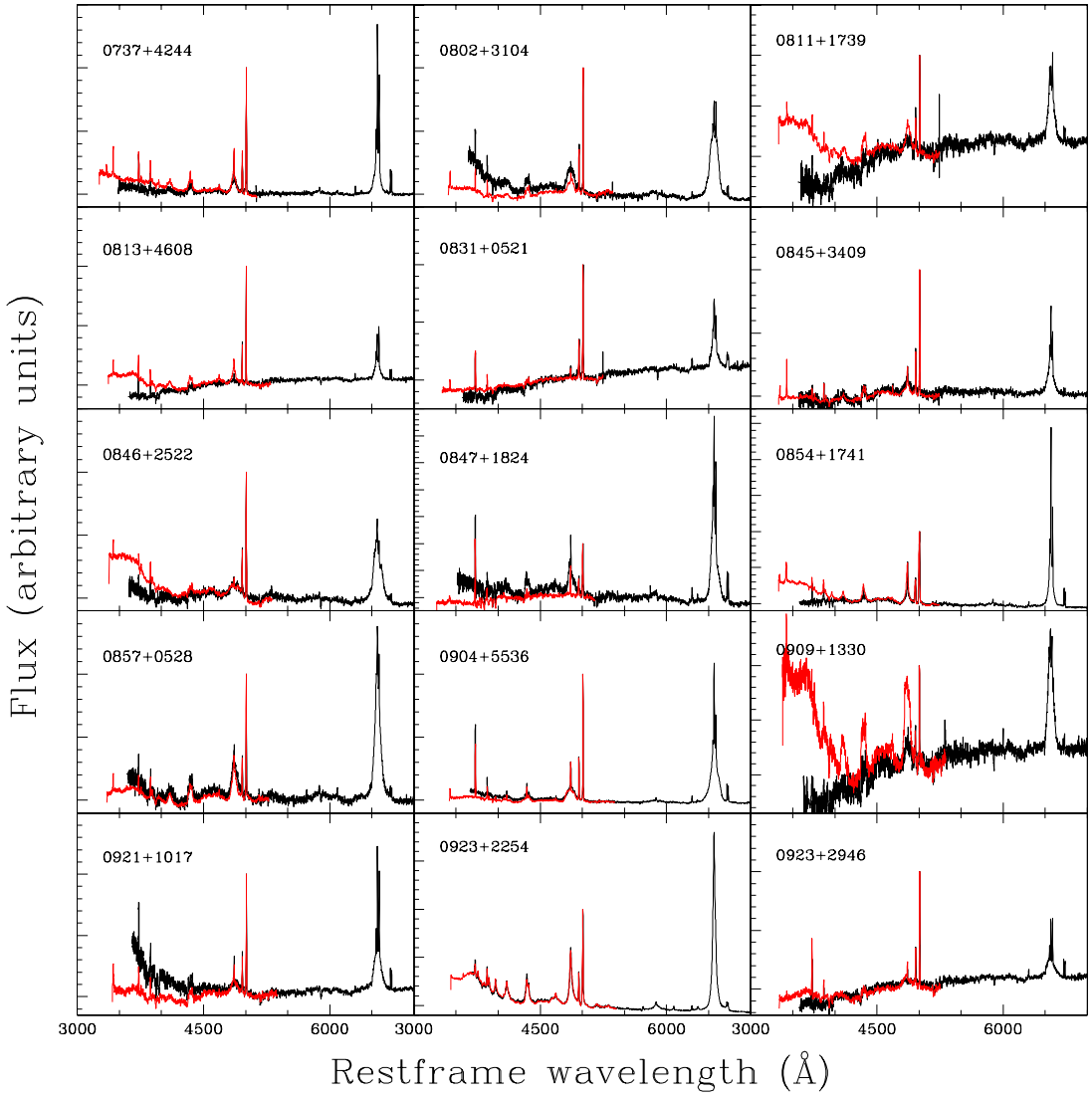

Figure A.2: Same as Figure A.1 but with 15 different objects.

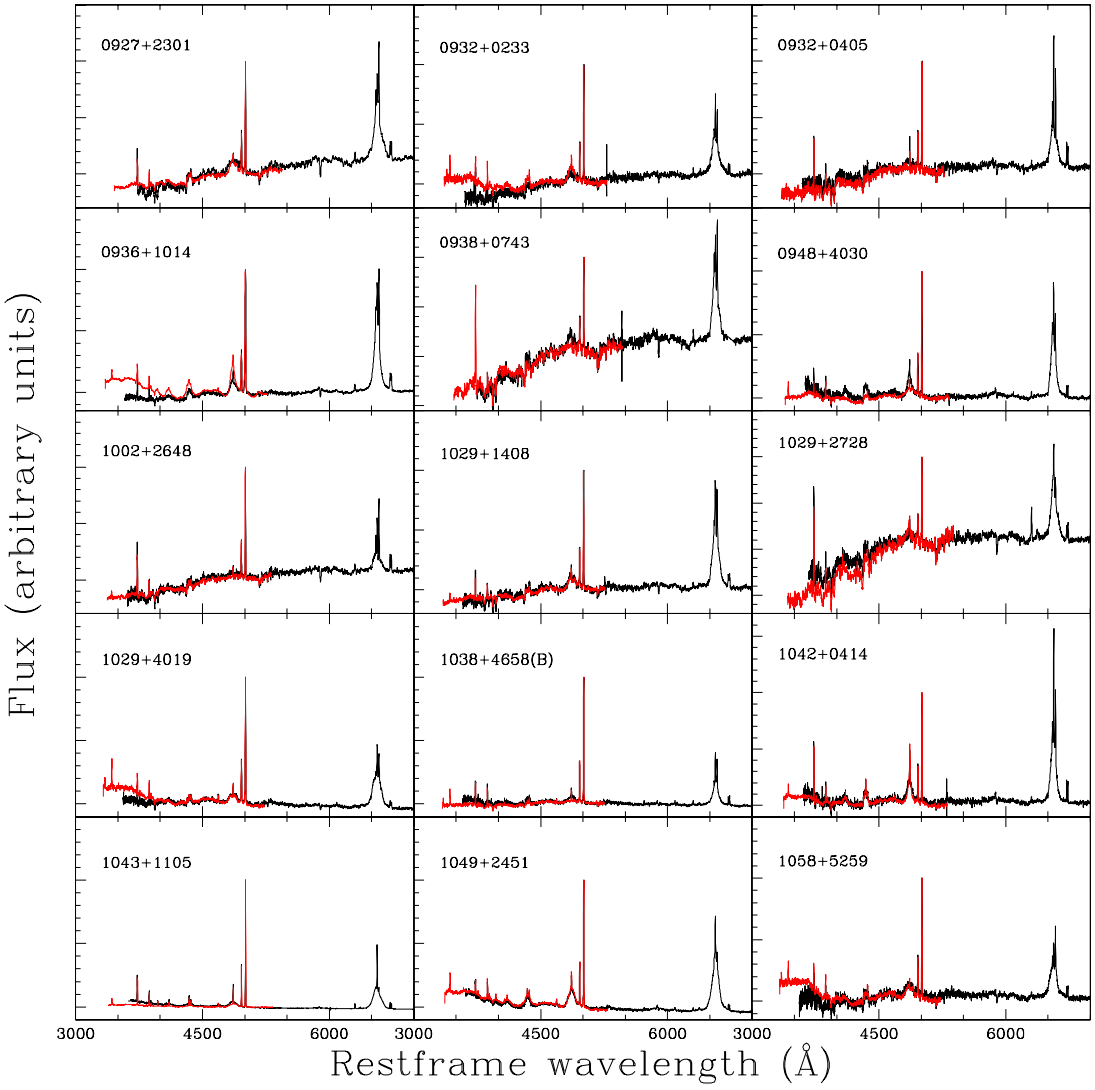

Figure A.3: Same as Figure A.1 but with 15 different objects.

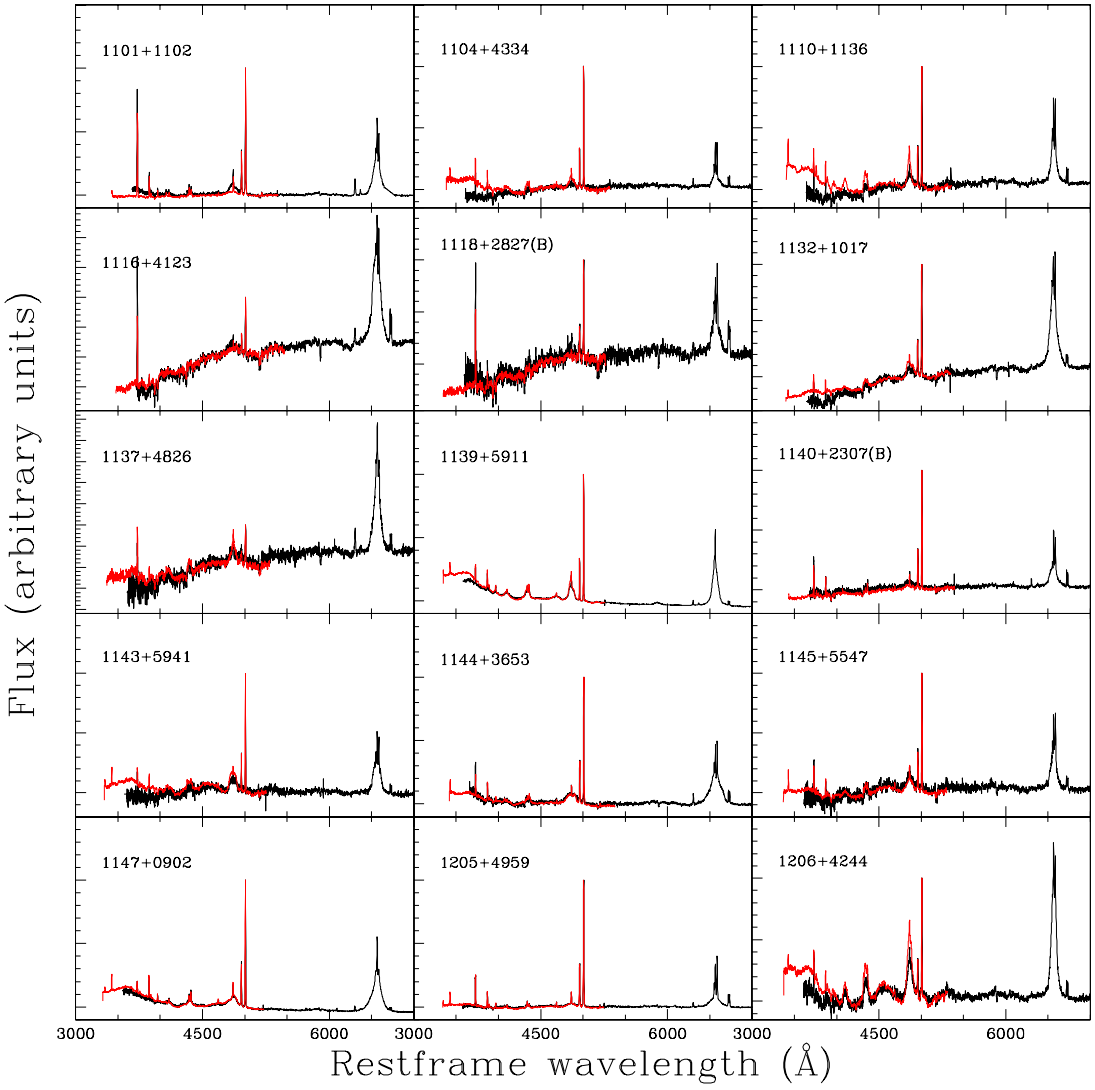

Figure A.4: Same as Figure A.1 but with 15 different objects.

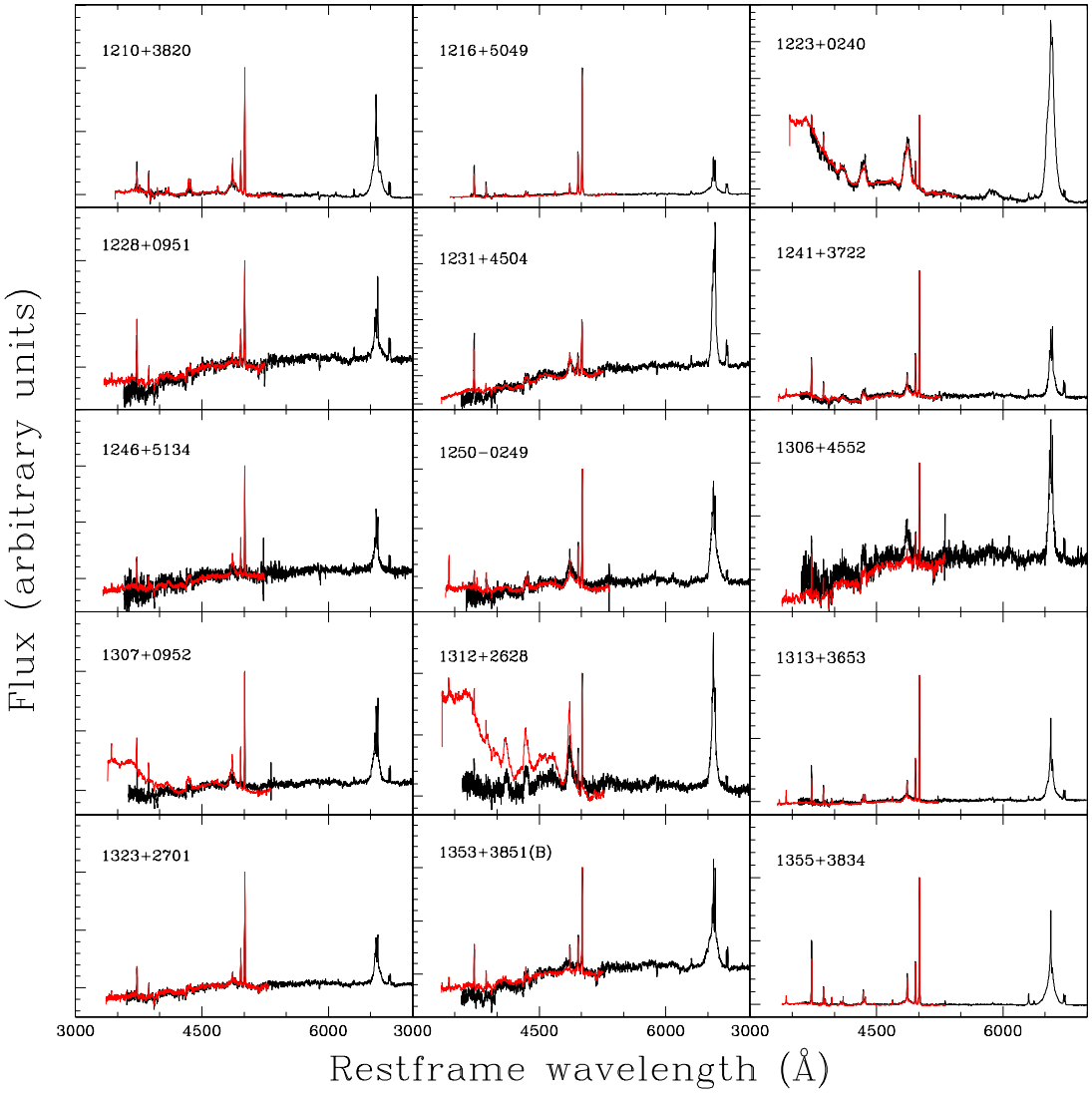

Figure A.5: Same as Figure A.1 but with 15 different objects.

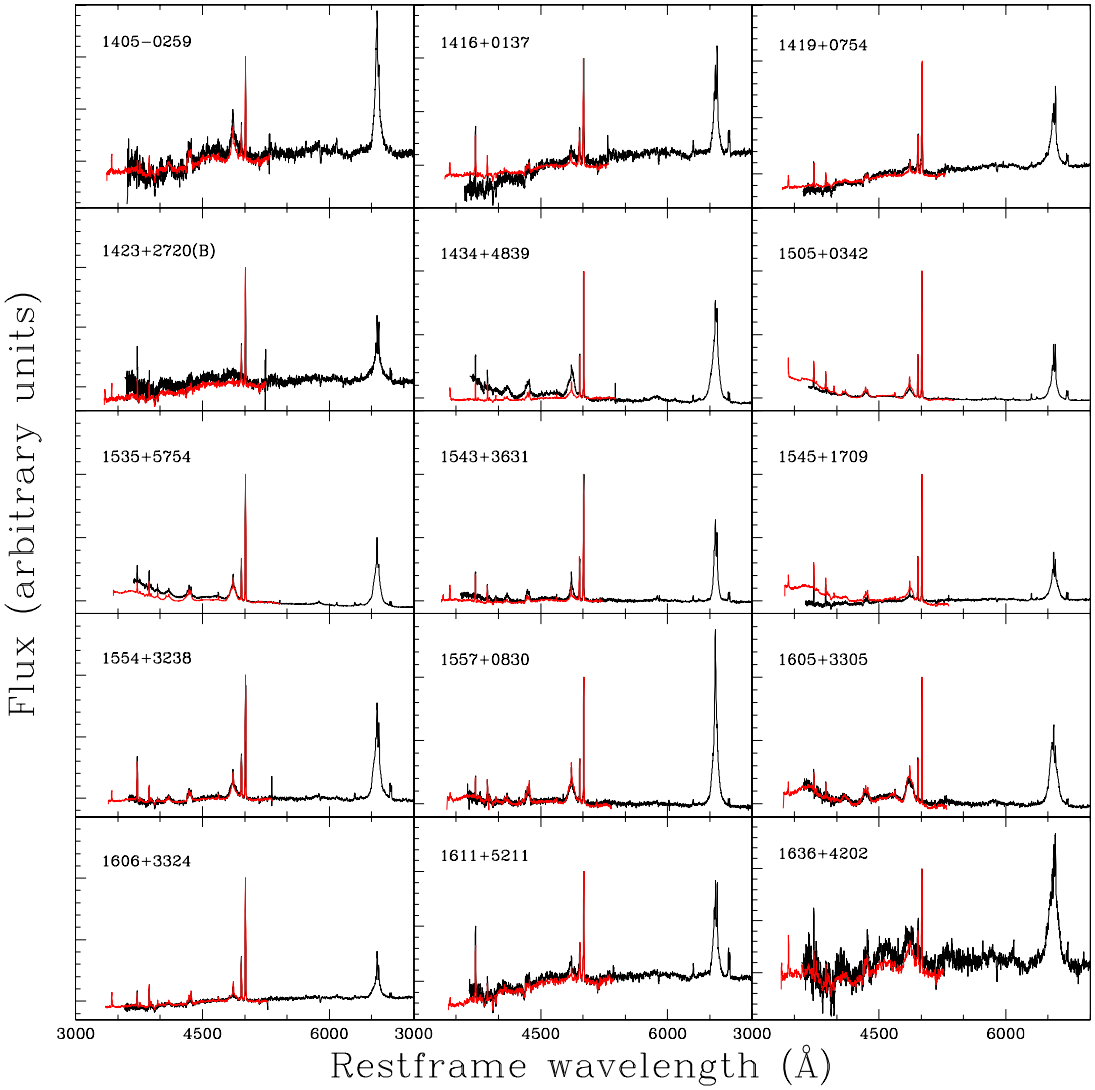

Figure A.6: Same as Figure A.1 but with 15 different objects.

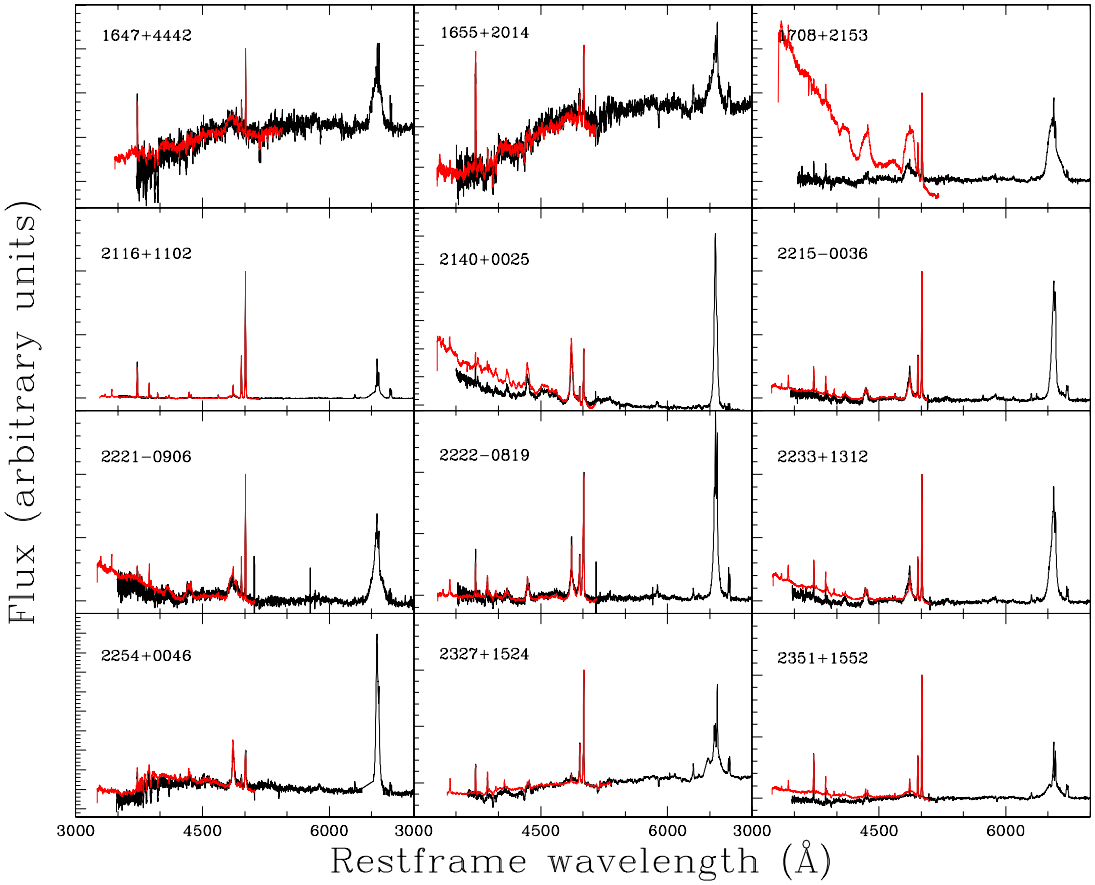

Figure A.7: Same as Figure A.1 but with 12 different objects.

A.2 Subtracted Spectra

This section overlays the subtracted SDSS and Keck spectra for every object in our sample to compare changes to the Hβ line.

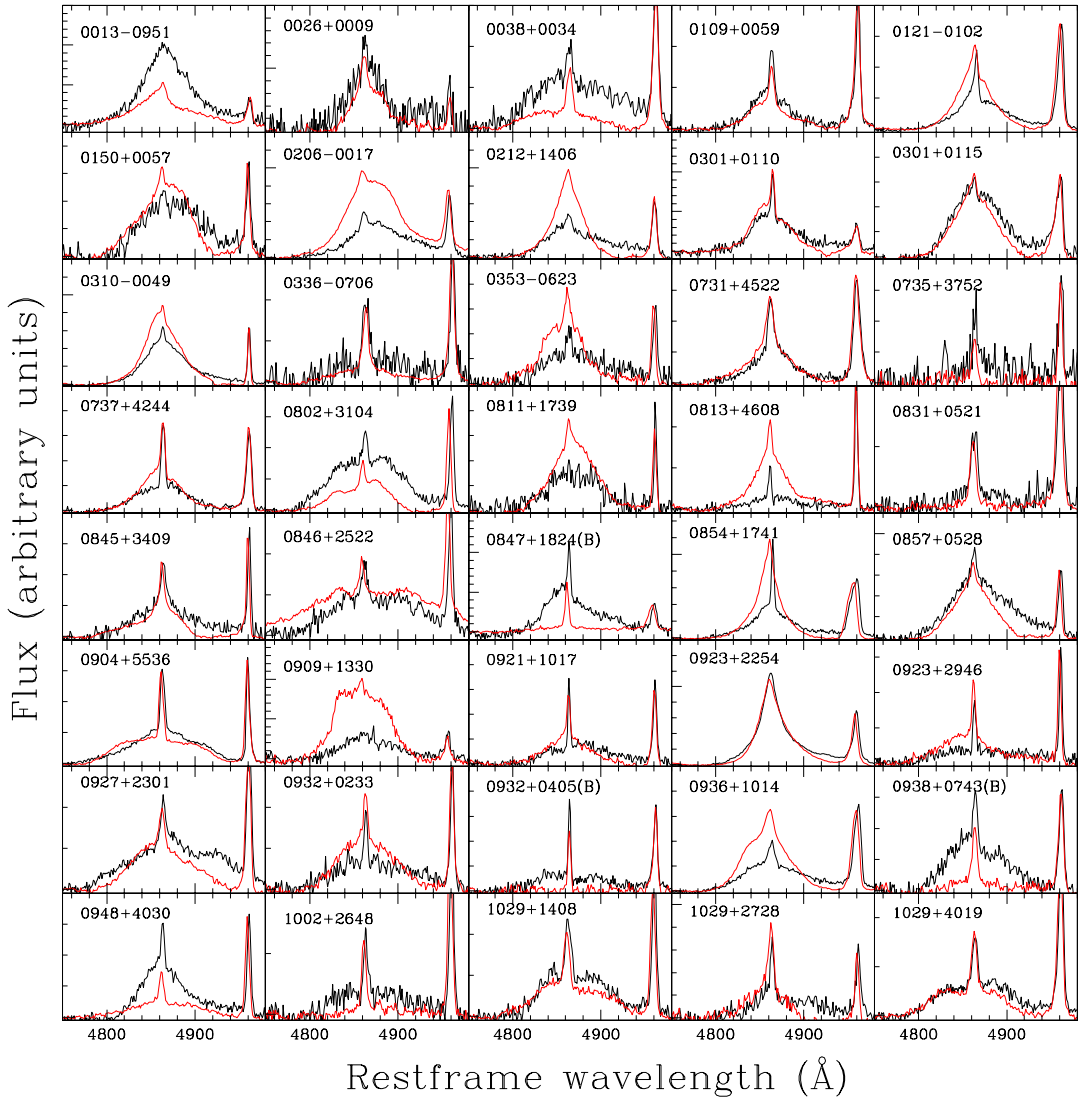

Figure A.8: 40 objects from the subtracted data. The black spectra is SDSS and the red spectra is Keck. The x-axis has a range of 4750-4980Å and adjusted the y-axis individually for each object to better see the difference in the Hβ line between Keck and SDSS. Although not visible on the plots, the 5007Å [OIII] line is normalized so that the peak is at 1 to accurately compare the Keck and SDSS Hβ lines. Note that the 4959Å [OIII] line has one third of the flux of the 5007Å [OIII] line.

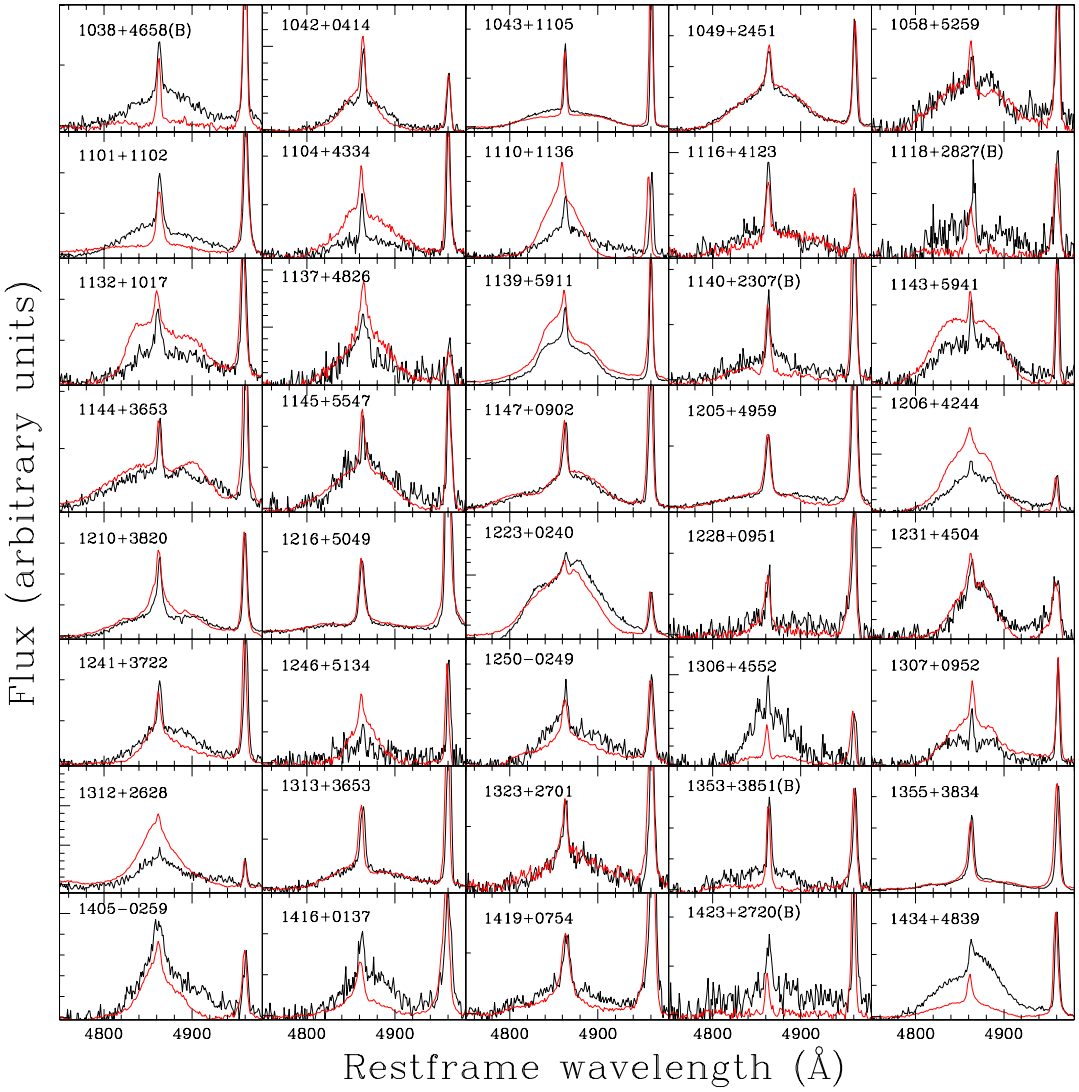

Figure A.9: The same as Figure A.8 but with 40 different objects.

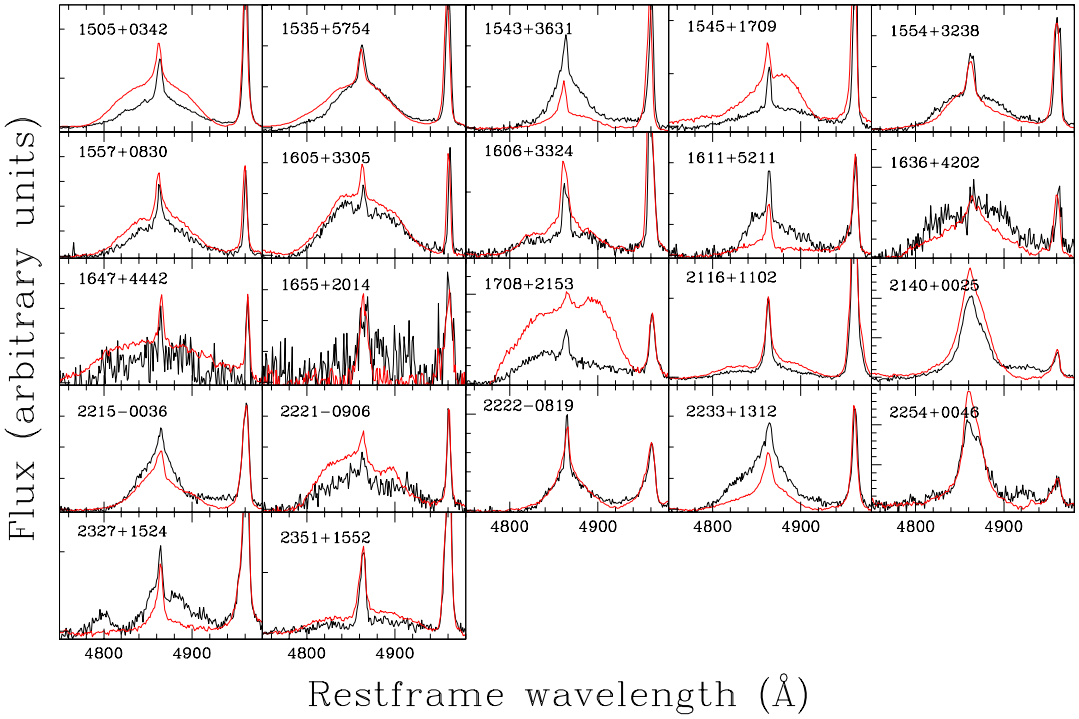

Figure A.10: The same as Figure A.8 but with 22 different objects.

Appendix B

Hβ Fitting

This section contains the fits to the Hβ and [OIII] (4959Å and 5007Å) lines as well as corresponding tables of values derived from the fitting for both Keck and SDSS spectra.

B.1 SDSS

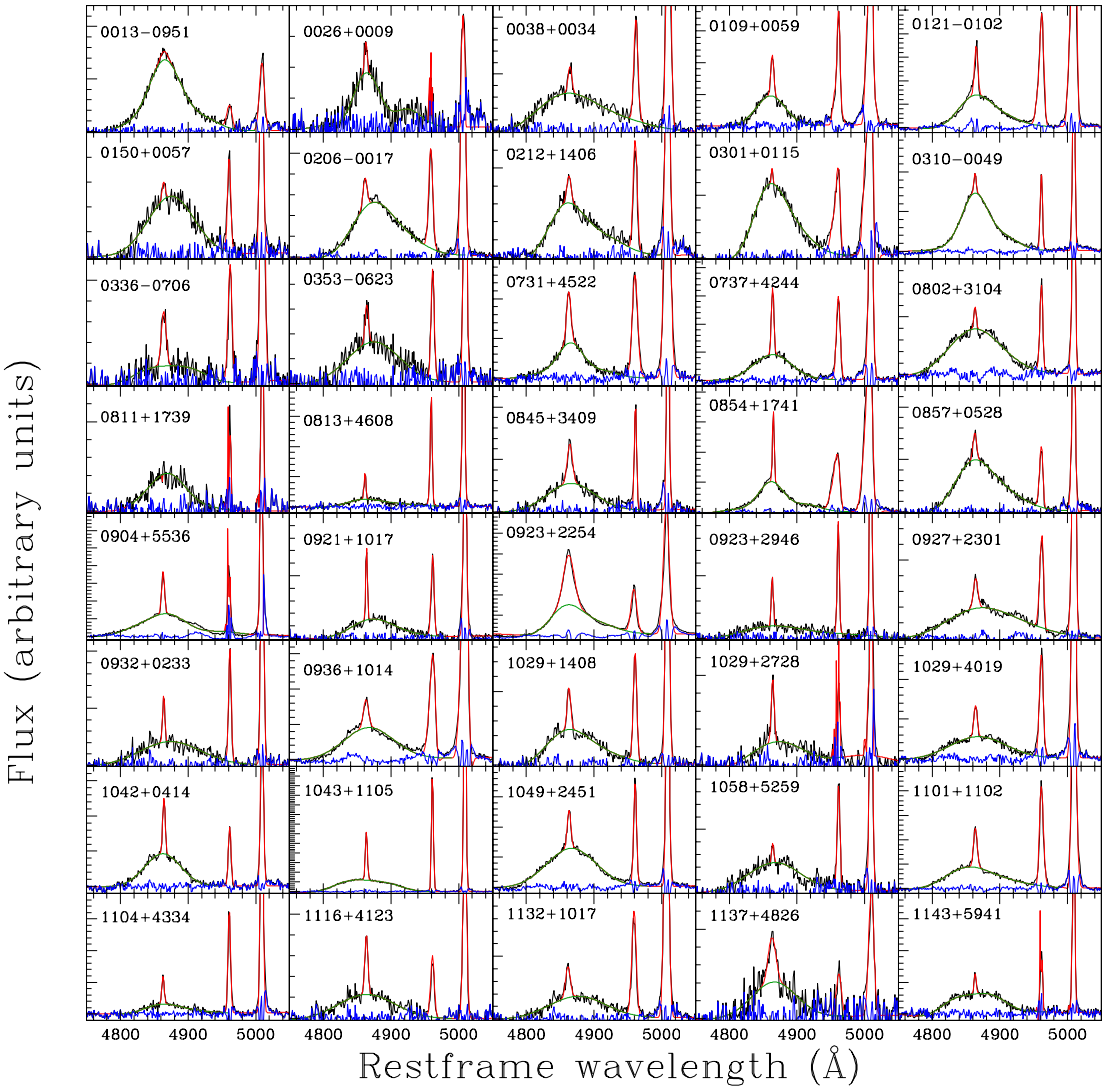

Figure B.1: Hβ fitting for 40 objects. The spectrum is shown in black, the fit to the data in red, the broad Hβ fit in green, and the residual in blue. The y-axis is adjusted individually for each object to better show the Hβ line and the first [OIII] line. Note that the 4959Å [OIII] line has one third of the flux of the 5007Å [OIII] line.

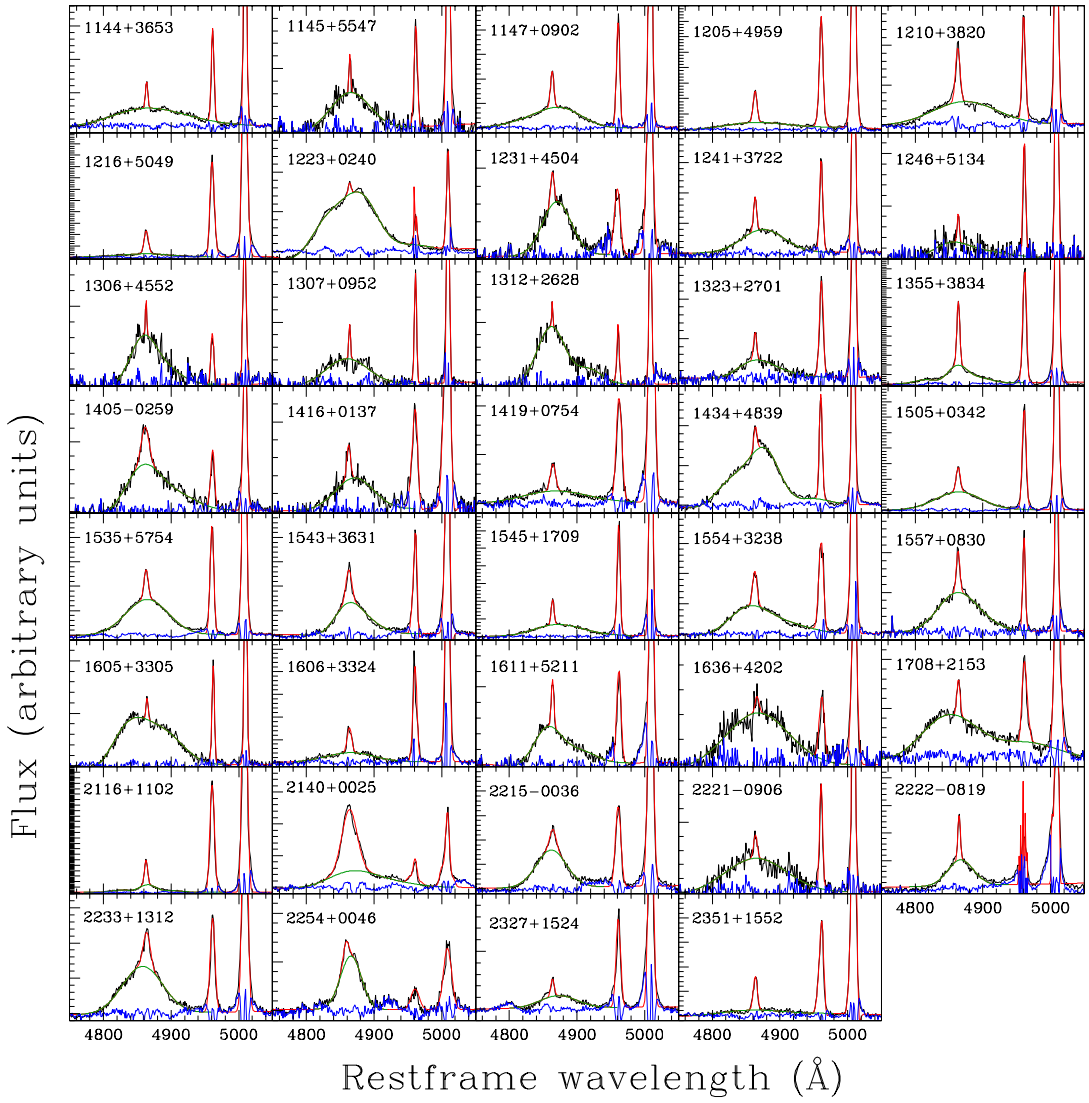

Figure B.2: The same as Figure B.1 but with 39 different objects.

SDSS Broad Hβ Fitting Data								
Object	I.D.	$\sigma_{H\beta}$ (km s^{-1})	log($M_{BH}/M_{\odot}$) (solar units)	FWHM (km s^{-1})	Second moment of data (km s^{-1})	λL_{5100} (10^{44} erg s^{-1})	Hβ/[OIII]	Hβ_{narrow}/ Hβ_{broad}
0013-0951	L71	2131	7.86	3796	2262	0.2251	0.19	0.02
0026+0009	L5	2248	7.38	2622	1856	0.0248	0.25	0.04
0038+0034	L73	3144	8.18	12147	3249	0.2084	0.08	0.04
0109+0059	L74	1302	7.24	2629	1468	0.1010	0.09	0.15
0121-0102	L11	1782	7.77	3036	1881	0.2903	0.10	0.13

Continued on next page

TableB.1– *Continued from previous page*

Object	I.D.	$\sigma_{H\beta}$ (km s^{-1})	$\log(M_{BH}/M_{\odot})$ (solar units)	FWHM (km s^{-1})	Second moment of data (km s^{-1})	λL_{5100} (10^{44} erg s^{-1})	Hβ/[OIII]	Hβ_{narrow}/ Hβ_{broad}
0150+0057	L76	2072	7.25	5798	1894	0.0196	0.06	0.02
0206-0017	L2	2149	8.08	4486	2356	0.5397	0.10	0.05
0212+1406	L77	2092	7.56	4279	2364	0.0693	0.09	0.05
0301+0115	L79	1750	7.60	3796	1815	0.1551	0.02	0.01
0310-0049	L80	1721	8.07	3105	1689	1.1722	0.09	0.02
0336-0706	L9	1944	7.43	7247	1737	0.0361	0.19	0.32
0353-0623	L6	2329	7.86	6557	2253	0.1600	0.12	0.06
0731+4522	L81	1898	7.54	2760	1858	0.0887	0.13	0.19
0737+4244	L83	1722	7.56	3727	1740	0.1410	0.18	0.18
0802+3104	L1	2290	7.65	5383	2445	0.0723	0.08	0.03
0811+1739	L114	1815	7.32	5245	1999	0.0423	0.03	0.01
0813+4608	L10	1925	7.40	4348	1828	0.0478	0.07	0.16
0845+3409	L126	2133	7.56	4210	2049	0.0639	0.27	0.16
0854+1741	L130	2014	7.85	2829	2066	0.2701	0.11	0.12
0857+0528	L19	2080	7.72	4417	2237	0.1347	0.16	0.04
0904+5536	L20	2414	7.75	5038	2388	0.0881	0.22	0.11
0921+1017	L22	1968	7.31	4210	1834	0.0296	0.17	0.15
0923+2254	L23	1865	7.71	3450	1791	0.1942	0.71	0.47
0923+2946	L138	3737	7.76	13251	3684	0.0194	0.14	0.10
0927+2301	L24	3289	7.32	7454	3383	0.0048	0.13	0.06
0932+0233	L26	2694	7.78	7109	2604	0.0688	0.11	0.07
0936+1014	L143	2232	7.69	4762	2455	0.0911	0.09	0.09
1029+1408	L155	2263	7.79	5452	2274	0.1325	0.13	0.09
1029+2728	L31	2301	7.26	4900	1962	0.0139	0.23	0.17
1029+4019	L156	2512	7.79	9111	2589	0.0932	0.09	0.09
1042+0414	L32	1630	7.21	3934	1495	0.0385	0.28	0.12
1043+1105	L33	1822	7.66	5383	1802	0.1709	0.14	0.20
1049+2451	L34	2228	7.92	5107	2235	0.2463	0.15	0.07
1058+5259	L162	2325	7.67	7040	2462	0.0749	0.05	0.03
1101+1102	L35	2405	7.68	4762	2292	0.0681	0.12	0.13
1104+4334	L36	1762	7.06	7247	1546	0.0159	0.08	0.18
1116+4123	L13	2546	7.05	8697	2477	0.0039	0.28	0.13
1132+1017	L14	2534	7.65	6350	2425	0.0494	0.11	0.11

Continued on next page

TableB.1– *Continued from previous page*

Object	I.D.	$\sigma_{H\beta}$ (km s^{-1})	$\log(M_{BH}/M_{\odot})$ (solar units)	FWHM (km s^{-1})	Second moment of data (km s^{-1})	λL_{5100} (10^{44} erg s^{-1})	Hβ/[OIII]	Hβ_{narrow}/ Hβ_{broad}
1137+4826	L39	2007	6.93	7868	1829	0.0057	0.52	0.21
1143+5941	L177	1845	7.54	8283	1816	0.0992	0.10	0.05
1144+3653	L15	3306	7.84	12216	3457	0.0415	0.08	.04
1145+5547	L41	1768	7.19	4486	1834	0.0265	0.07	0.05
1147+0902	L180	2307	8.20	4831	2435	0.6902	0.11	0.12
1205+4959	L187	3003	8.10	10560	2994	0.1768	0.10	0.21
1210+3820	L43	2830	7.80	5798	2879	0.0618	0.23	0.16
1216+5049	L44	2070	7.39	8006	2088	0.0349	0.08	0.69
1223+0240	L45	2133	7.04	5107	2083	0.0071	0.12	0.01
1231+4504	L196	1301	7.16	6212	1792	0.0730	0.10	0.07
1241+3722	L197	1929	7.56	4693	1744	0.0915	0.12	0.11
1246+5134	L202	2191	7.49	8559	2096	0.0438	0.07	0.09
1306+4552	L47	1520	6.97	3727	1481	0.0184	0.11	0.03
1307+0952	L48	1905	7.36	5038	1932	0.0408	0.08	0.05
1312+2628	L204	1839	7.64	2898	1765	0.1542	0.07	0.01
1323+2701	L49	1758	7.18	3934	1728	0.0257	0.08	0.13
1355+3834	L50	1747	7.49	2138	1627	0.0968	0.15	0.36
1405-0259	L51	1960	7.22	5038	2001	0.0205	0.44	0.15
1416+0317	L52	1714	7.37	3519	1734	0.0640	0.08	0.08
1419+0754	L53	2827	7.95	7523	2605	0.1157	0.08	0.18
1434+4839	L54	2167	7.86	4003	2089	0.2105	0.08	0.03
1505+0342	L56	2067	7.96	4624	2063	0.3817	0.08	0.12
1535+5754	L57	1929	7.83	4417	2034	0.2871	0.10	0.09
1543+3631	L214	1439	7.52	2622	1639	0.2286	0.17	0.19
1545+1709	L58	2188	7.60	8214	1981	0.0697	0.07	0.13
1554+3238	L59	2257	7.77	8764	2343	0.1252	0.12	0.11
1557+0830	L60	1876	7.45	3865	1931	0.0632	0.19	0.09
1605+3305	L61	1877	7.78	5521	1980	0.2544	0.06	0..02
1606+3324	L62	2080	7.55	6005	1949	0.0673	0.10	0.25
1611+5211	L63	1712	7.34	7178	1654	0.0558	0.11	0.10
1636+4202	L205	2817	7.96	5867	2952	0.1250	0.07	0.02
1708+2153	L91	3921	7.61	12838	3961	0.2765	0.09	0.03
2116+1102	L96	1611	7.61	7178	475	0.2199	0.05	0.43

Continued on next page

TableB.1– *Continued from previous page*

Object	I.D.	$\sigma_{\mathrm{H}\beta}$ (km s^{-1})	$\log(M_{\mathrm{BH}}/M_{\odot})$ (solar units)	FWHM (km s^{-1})	Second moment of data (km s^{-1})	λL_{5100} (10^{44} erg s^{-1})	Hβ/[OIII]	Hβ_{narrow}/ Hβ_{broad}
2140+0025	L99	2516	8.23	6143	2392	0.5846	2.25	1.01
2215-0036	L100	1368	7.45	2967	1527	0.2019	0.11	0.12
2221-0906	L102	2747	7.90	7109	2710	0.1035	0.08	0.04
2222-0819	L103	1165	7.28	2622	1039	0.1768	0.16	0.18
2233+1312	L106	1823	7.84	4279	1810	0.3679	0.18	0.13
2254+0046	L108	949	7.34	2000	1231	0.4806	0.21	0.10
2327+1524	L70	1658	7.39	6419	1955	0.0791	0.05	0.13
2351+1552	L109	2921	8.06	9732	2917	0.1651	0.11	0.30

Table B.1: This is a table of 79 SDSS objects where the Hβ line was fit showing the values: $\sigma_{\mathrm{H}\beta}$, $\log(M_{\mathrm{BH}}/M_{\odot})$, FWHM of the broad H$\beta$ line, second moment of the data to the broad Hβ line, continuum luminosity at 5100Å, Hβ/[OIII] flux ratio, and Hβ_{narrow}/Hβ_{broad} flux ratio. The uncertainty of $\log(M_{\mathrm{BH}}/M_{\odot})$ is 0.4 dex, the uncertainty for λL_{5100} is 0.1 dex, the uncertainty for the velocities is $\sim$10%, and the uncertainty for the fluxes is $\sim$5%.

B.2 Keck

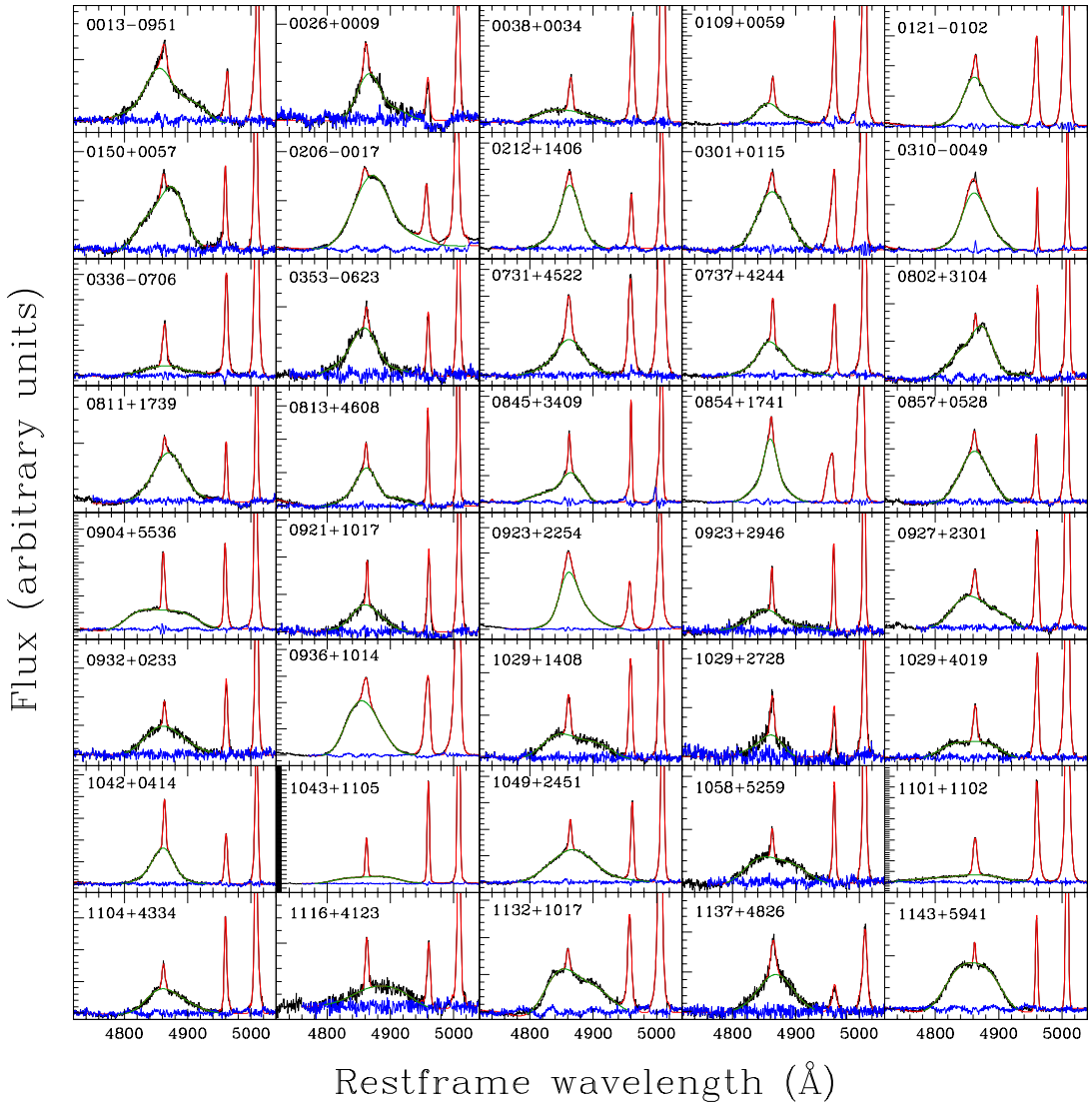

Figure B.3: Hβ fitting for 40 objects. The spectrum is shown in black, the fit to the data in red, the broad Hβ fit in green, and the residual in blue. The y-axis is adjusted individually for each object to better show the Hβ line and the first [OIII] line. Note that the 4959Å [OIII] line has one third of the flux of the 5007Å [OIII] line.

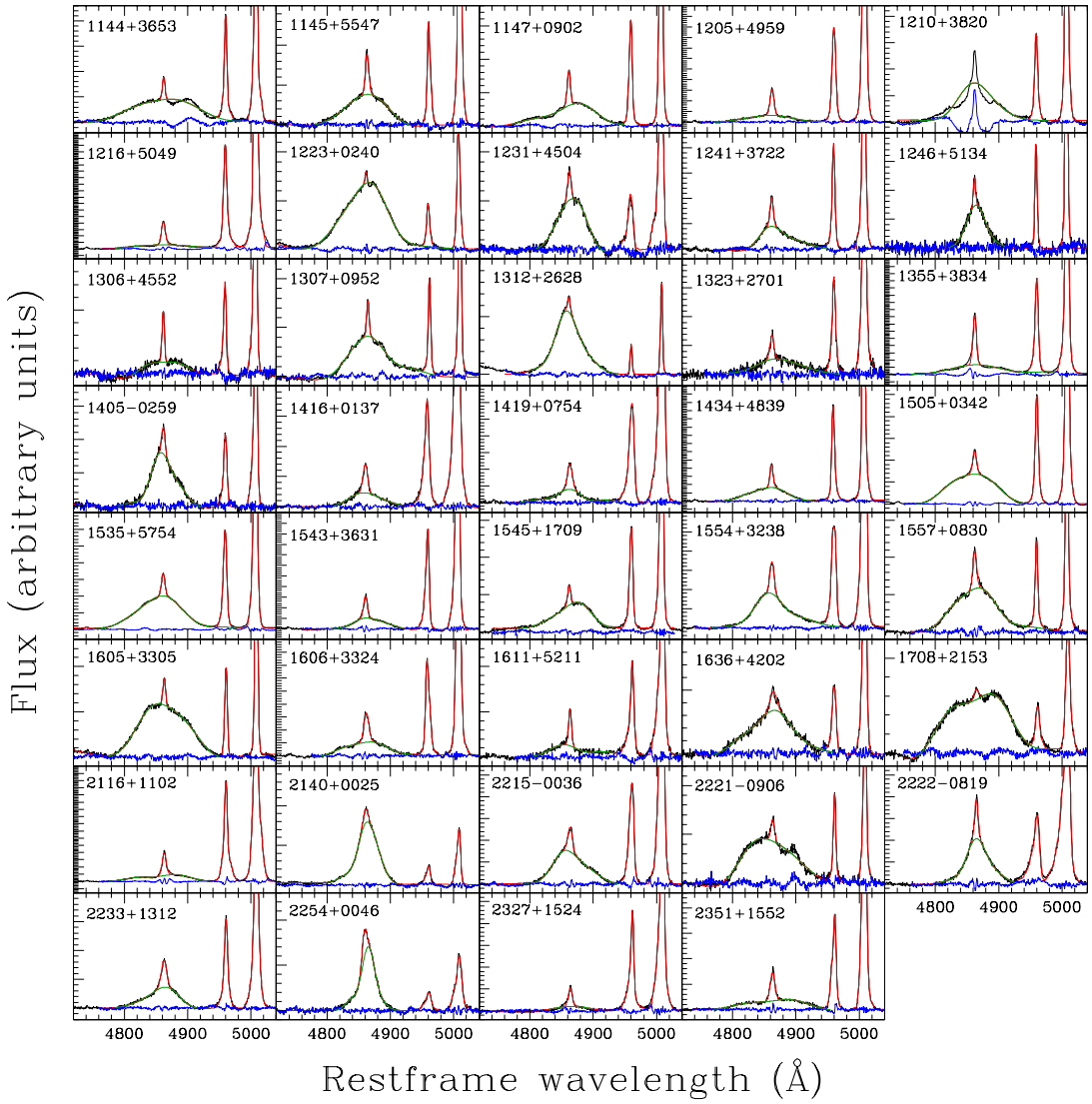

Figure B.4: The same as Figure B.3 but with 39 different objects.

Keck Broad Hβ Fitting Data								
Object	I.D.	$\sigma_{H\beta}$ (km s^{-1})	$\log(M_{BH}/M_{\odot})$ (solar units)	FWHM (km s^{-1})	Second moment of data (km s^{-1})	λL_{5100} (10^{44} erg s^{-1})	Hβ/[OIII]	Hβ_{narrow}/ Hβ_{broad}
0013-0951	L71	1996	7.80	3658	2016	0.2251	0.23	0.07
0026+0009	L5	1456	7.00	2671	1522	0.0248	0.27	0.10
0038+0034	L73	1849	7.72	5187	1848	0.2084	0.11	0.26
0109+0059	L74	1307	7.24	2631	1323	0.1010	0.07	0.17
0121-0102	L11	1316	7.50	2541	1299	0.2903	0.06	0.06

Continued on next page

TableB.2– *Continued from previous page*

Object	I.D.	$\sigma_{H\beta}$ (km s^{-1})	$\log(M_{BH}/M_{\odot})$ (solar units)	FWHM (km s^{-1})	Second moment of data (km s^{-1})	λL_{5100} (10^{44} erg s^{-1})	Hβ/[OIII]	Hβ_{narrow}/ Hβ_{broad}
0150+0057	L76	1587	7.02	3970	1579	0.0196	0.10	0.04
0206-0017	L2	1990	8.01	4051	2023	0.5397	0.08	0.02
0212+1406	L77	1175	7.05	2229	1173	0.0693	0.10	0.04
0301+0115	L79	1365	7.38	3179	1353	0.1551	0.06	0.05
0310-0049	L80	1307	7.83	2623	1296	1.1722	0.06	0.01
0336-0706	L9	1754	7.26	4110	1741	0.0361	0.15	0.41
0353-0623	L6	1694	7.58	3179	1695	0.1600	0.11	0.04
0731+4522	L81	1664	7.42	3307	1632	0.0887	0.14	0.18
0737+4244	L83	1683	7.54	2998	1691	0.1410	0.14	0.11
0802+3104	L1	1749	7.42	3618	1803	0.0723	0.07	0.07
0811+1739	L114	1505	7.16	3277	1493	0.0423	0.12	0.03
0813+4608	L10	1693	7.29	2468	1744	0.0478	0.10	0.06
0845+3409	L126	1508	7.26	4864	1497	0.0639	0.15	0.14
0854+1741	L130	1097	7.33	1639	1099	0.2701	0.07	0.06
0857+0528	L19	1392	7.37	3228	1394	0.1347	0.12	0.05
0904+5536	L20	2023	7.59	6220	1991	0.0881	0.21	0.19
0921+1017	L22	1455	7.05	3436	1479	0.0296	0.12	0.12
0923+2254	L23	1335	7.42	2403	1360	0.1942	0.19	0.09
0923+2946	L138	2183	7.30	4106	2216	0.0194	0.15	0.11
0927+2301	L24	1955	6.87	4845	1971	0.0048	0.09	0.07
0932+0233	L26	1753	7.41	4444	1732	0.0688	0.10	0.06
0936+1014	L143	1474	7.32	3594	1498	0.0911	0.10	0.08
1029+1408	L155	2029	7.69	5991	2048	0.1325	0.14	0.15
1029+2728	L31	1162	6.67	3033	1129	0.0139	0.28	0.27
1029+4019	L156	1858	7.53	5648	1860	0.0932	0.11	0.20
1042+0414	L32	1251	6.98	3934	1495	0.0385	0.28	0.15
1043+1105	L33	1909	7.70	6188	1909	0.1709	0.12	0.31
1049+2451	L34	2225	7.92	4743	2241	0.2463	0.12	0.06
1058+5259	L162	1938	7.52	5196	1987	0.0749	0.09	0.07
1101+1102	L35	2900	7.84	6546	2940	0.0681	0.12	0.29
1104+4334	L36	1713	7.04	3881	1755	0.0159	0.09	0.09
1116+4123	L13	2104	6.88	6172	2145	0.0039	0.22	0.16
1132+1017	L14	1965	7.43	5497	1976	0.0494	0.05	0.04

Continued on next page

TableB.2– *Continued from previous page*

Object	I.D.	$\sigma_{H\beta}$ (km s^{-1})	$\log(M_{BH}/M_{\odot})$ (solar units)	FWHM (km s^{-1})	Second moment of data (km s^{-1})	λL_{5100} (10^{44} erg s^{-1})	Hβ/[OIII]	Hβ_{narrow}/ Hβ_{broad}
1137+4826	L39	1585	6.73	3938	1594	0.0057	0.41	0.13
1143+5941	L177	1752	7.50	5082	1761	0.0992	0.05	0.02
1144+3653	L15	2551	7.61	6998	2675	0.0415	0.06	0.05
1145+5547	L41	1813	7.21	4320	1808	0.0265	0.13	0.11
1147+0902	L180	2320	8.20	4350	2320	0.6902	0.11	0.10
1205+4959	L187	2060	7.77	5047	2113	0.1768	0.09	0.34
1210+3820	L43	2376	7.65	5086	2369	0.0618	0.25	0.19
1216+5049	L44	1585	7.16	2480	1922	0.0349	0.07	0.48
1223+0240	L45	2037	7.00	4668	2136	0.0071	0.05	0.01
1231+4504	L196	1163	7.07	3032	1176	0.0730	0.11	0.08
1241+3722	L197	1541	7.36	3209	1624	0.0915	0.10	0.15
1246+5134	L202	989	6.80	2214	2096	0.0438	0.08	0.08
1306+4552	L47	1384	6.89	4062	1354	0.0184	0.13	0.29
1307+0952	L48	2047	7.42	3701	2013	0.0408	0.11	0.06
1312+2628	L204	1430	7.42	2678	1397	0.1542	0.21	0.03
1323+2701	L49	2133	7.34	6165	2105	0.0257	0.08	0.13
1355+3834	L50	3110	7.99	3397	3102	0.0968	0.17	0.24
1405-0259	L51	1341	6.89	2687	1332	0.0205	0.11	0.07
1416+0317	L52	1445	7.22	3317	1418	0.0640	0.07	0.29
1419+0754	L53	1931	7.62	2869	1998	0.1157	0.07	0.28
1434+4839	L54	1571	7.58	3573	1541	0.2105	0.08	0.16
1505+0342	L56	1823	7.85	5253	1804	0.3817	0.08	0.08
1535+5754	L57	2018	7.87	4716	2081	0.2871	0.07	0.06
1543+3631	L214	1451	7.53	2906	1439	0.2286	0.07	0.23
1545+1709	L58	1603	7.33	3773	1664	0.0697	0.06	0.07
1554+3238	L59	1987	7.66	3224	2026	0.1252	0.09	0.11
1557+0830	L60	2018	7.51	4385	2041	0.0632	0.18	0.09
1605+3305	L61	1980	7.83	5531	1980	0.2544	0.10	0.03
1606+3324	L62	1736	7.39	4737	1736	0.0673	0.12	0.27
1611+5211	L63	1842	7.40	2091	1854	0.0558	0.09	0.27
1636+4202	L205	2183	7.74	4687	2199	0.1250	0.20	0.10
1708+2153	L91	2279	7.97	6765	2339	0.2765	0.08	0.02
2116+1102	L96	1949	7.78	3010	1931	0.2199	0.07	0.36

Continued on next page

TableB.2– *Continued from previous page*

Object	I.D.	$\sigma_{\mathrm{H}\beta}$ (km s^{-1})	$\log(M_{\mathrm{BH}}/M_{\odot})$ (solar units)	FWHM (km s^{-1})	Second moment of data (km s^{-1})	λL_{5100} (10^{44} erg s^{-1})	Hβ/[OIII]	Hβ_{narrow}/ Hβ_{broad}
2140+0025	L99	1085	7.50	2111	1089	0.5846	0.29	0.05
2215-0036	L100	1559	7.56	3285	1571	0.2019	0.07	0.11
2221-0906	L102	1955	7.60	5627	1937	0.1035	0.10	0.04
2222-0819	L103	1333	7.40	2221	1336	0.1768	0.09	0.13
2233+1312	L106	1478	7.66	3161	1485	0.3679	0.13	0.23
2254+0046	L108	924	7.32	1492	937	0.4806	0.34	0.12
2327+1524	L70	875	6.84	1556	901	0.0791	0.04	0.43
2351+1552	L109	2343	7.87	5346	2288	0.1651	0.11	0.27

Table B.2: This is a table of 79 Keck objects where the Hβ line was fit showing the values: $\sigma_{\mathrm{H}\beta}$, $\log(M_{\mathrm{BH}}/M_{\odot})$, FWHM of the broad H$\beta$ line, second moment of the data to the broad Hβ line, continuum luminosity at 5100Å, Hβ/[OIII] flux ratio, and Hβ_{narrow}/Hβ_{broad} flux ratio. The uncertainty of $\log(M_{\mathrm{BH}}/M_{\odot})$ is 0.4 dex, the uncertainty for λL_{5100} is 0.1 dex, the uncertainty for the velocities is $\sim$10%, and the uncertainty for the fluxes is $\sim$5%.

Appendix C

Continuum Powerlaw Fitting

This section contains the values of the continuum powerlaw exponent (b) for all 102 objects for both SDSS and Keck spectra. The continuum is modeled after the equation $y = Ax^b$. The powerlaw exponent is important because it changes the shape of the continuum.

Continuum Powerlaw Exponent Fitting Data			
Object	I.D.	SDSS values	Keck values
0013-0951	L71	−1.99	−1.34
0026+0009	L5	−0.34	−1.16
0038+0034	L73	−2.55	−2.14
0109+0059	L74	−1.29	−2.42
0121-0102	L11	−2.21	−3.49
0150+0057	L76	−1.49	−2.91
0206-0017	L2	−3.19	−4.86
0212+1406	L77	−0.06	−0.98
0301+0110	L78	−1.34	−1.54
0301+0115	L79	−1.57	−1.94
0310-0049	L80	−1.91	−2.82
0336-0706	L9	2.07	0.73
0353-0623	L6	−1.37	−2.20
0731+4522	L81	−0.39	−1.08
0735+3752	L82	0.10	0.35
0737+4244	L83	−1.84	−2.77
0802+3104	L1	−3.60	−4.08
0811+1739	L114	−0.90	−4.93
0813+4608	L10	−0.06	−6.33

Continued on next page

TableC.1– *Continued from previous page*

Object	I.D.	SDSS values	SDSS values
0831+0521	L208	1.82	−1.41
0845+3409	L126	−1.85	−3.01
0846+2522	L4	−1.81	−3.25
0847+1842	L8	−2.40	−0.87
0854+1741	L130	−1.06	−4.07
0857+0528	L19	−2.37	−4.15
0904+5536	L20	−2.16	−1.79
0909+1330	L21	−0.98	−5.15
0921+1017	L22	−4.69	−3.98
0923+2254	L23	−4.24	−4.65
0923+2946	L138	−1.23	−3.49
0927+2301	L24	−2.64	−0.35
0932+0233	L26	−0.68	−4.28
0932+0405	L27	−1.92	−2.56
0936+1014	L143	0.06	−4.71
0938+0743	L28	−2.16	−4.63
0948+4030	L29	−2.78	−2.54
1002+2648	L30	−2.71	−0.68
1029+1408	L155	−1.14	−1.26
1029+2728	L31	−4.33	−3.17
1029+4019	L156	−1.60	−3.86
1038+4658	L157	−1.76	−2.65
1042+0414	L32	−2.31	−2.72
1043+1105	L33	−3.04	−3.29
1049+2451	L34	−2.68	−3.49
1058+5259	L162	−3.25	−4.82
1101+1102	L35	−2.24	−1.62
1104+4334	L36	−1.22	−5.07
] 1110+1136	L37	−1.84	−5.83
1116+4123	L13	−3.21	1.33
1118+2827	L38	−2.33	−1.01
1132+1017	L14	0.67	0.36
1137+4826	L39	−1.15	−4.02
1139+5911	L174	−3.75	−5.17

Continued on next page

TableC.1– *Continued from previous page*

Object	I.D.	SDSS values	SDSS values
1140+2307	L40	−1.75	−0.81
1143+5941	L177	−1.43	−1.80
1144+3653	L15	−3.14	−3.66
1145+5547	L41	−3.08	−4.00
1147+0902	L180	−3.37	−3.96
1205+4959	L187	−2.04	−4.39
1206+4244	L42	−2.86	−3.33
1210+3820	L43	−1.41	−1.19
1216+5049	L44	−2.98	−1.00
1223+0240	L45	−3.88	−4.56
1228+0951	L210	−1.53	−3.36
1231+4504	L196	1.05	0.75
1241+3722	L197	−2.76	−4.16
1246+5134	L202	−1.19	−1.03
1250-0249	L46	−1.14	−1.62
1306+4552	L47	−2.53	−1.20
1307+0952	L48	−2.02	−5.11
1312+2628	L204	−1.29	−3.77
1313+3653	L213	−1.08	−1.50
1323+2701	L49	−2.43	−1.59
1353+3951	L207	−1.46	−2.63
1355+3834	L50	−1.87	−1.89
1405-0259	L51	−1.56	−2.06
1416+0317	L52	0.05	−1.98
1419+0754	L53	−0.17	0.31
1423+2720	L209	−2.25	−2.00
1434+4839	L54	−3.00	−1.03
1505+0342	L56	−3.20	−5.29
1535+5754	L57	−3.39	−2.29
1543+3631	L214	−2.25	−3.97
1545+1709	L58	−2.14	−3.69
1554+3238	L59	−1.46	−1.86
1557+0830	L60	−1.33	−1.58
1605+3305	L61	−3.04	−3.38

Continued on next page

TableC.1– *Continued from previous page*

Object	I.D.	SDSS values	SDSS values
1606+3324	L62	−0.49	−0.79
1611+5211	L63	−2.24	−0.24
1636+4202	L205	−1.97	−3.69
1647+4442	L64	−2.40	−1.61
1655+2014	L88	−0.29	−0.82
1708+2153	L91	−1.14	−3.93
2116+1102	L96	−2.33	−1.87
2140+0025	L99	−1.61	−2.11
2215-0036	L100	−1.86	−3.48
2221-0906	L102	−2.92	−3.85
2222-0819	L103	−1.34	−1.51
2233+1312	L106	−2.05	−3.68
2254+0046	L108	−0.01	−0.23
2327+1524	L70	−1.89	−0.52
2351+1552	L109	−1.45	−2.76

Table C.1: Continuum powerlaw exponent fitting data for all SDSS and Keck objects in our sample. The estimated uncertainty is ∼10%.